QATAR UNIVERSITY

COLLEGE OF ENGINEERING

INVESTIGATING THE POTENTIAL OF RECYCLING FLARED HYDROCARBON GAS IN AN INDUSTRIAL BURNER

BY

FAHD M. MOHAMMED

A Thesis Submitted to

the Faculty of the College of

Engineering

in Partial Fulfillment

of the Requirements

for the Degree of

Masters of Science in Mechanical Engineering

June 2018

COMMITTEE PAGE

The members of the Committee approve the Thesis of Fahd M. Mohammed defended on 20/05/2018.

_____

Dr. Samer F. Ahmed
Thesis Supervisor

_____

Dr. Fadwa T. Eljack
Thesis Supervisor

_____

Saud Ghani
Internal Examiner

_____

Mahmoud M El-Halwagi
External Examiner

_____

Riyadh Al-Raoush
Committee Chairman

Approved:

_____

Khalifa Al-Khalifa, Dean, College of Engineering

ABSTRACT

MOHAMMED, FAHD, M., Masters : June : [2018:],

Masters of Science in Mechanical Engineering

Title: Investigating the Potential of Recycling Flared Hydrocarbon Gas in an Industrial Burner

Supervisor of Thesis: Samer, F., Ahmed and Fadwa, T., Eljack.

Flare gas is considered a global environmental concern. Flaring contributes to wasting limited material and energy resources, economic loss and greenhouse gas emissions. Utilizing flared gas as fuel feed to industrial cracking furnaces grants advantages in terms of fuel economy and emissions reduction. This work presents the results obtained by ANSYS fluent simulation of a flared hydrocarbon gas utilized in a steam cracking furnace of ethylene process. The work focused on simulating the flue gas side in a steam cracking furnace of the ethylene process when combusting hydrocarbons flare gas. The flared stream assumed to be inlet from both primary and secondary staged fuel nozzles. The simulation results illustrate the detailed temperature profiles along the furnace flue gas side. It also investigates the influence of flare stream composition and Wobbe Index (WI) influence on temperature profile.

DEDICATION

In the name of Allah, the most merciful, the most compassionate all praise be to Allah, the lord of the worlds; and prayers and peace be upon Mohamed his servant and messenger. I dedicate this work to my family, who has been affected in every way possible by this quest. Your unwavering support and motivation throughout this thesis project was incredible. I love you

ACKNOWLEDGMENTS

I would like to express my sincere gratitude to my advisors Dr. Samer Ahmed and Dr. Fadwa Eljack for the continuous support of my thesis study. I am also grateful to Eng.Mohammed Basiony for sharing his office and resources with me during this work. I am using this opportunity to express my gratitude to all colleagues who supported me throughout the course. Last but not the least; I would like to thank Eng.Tarek Shaban for dedicating his time to help me and for supporting me spiritually throughout accomplishing this thesis.

TABLE OF CONTENTS

LIST OF TABLES

LIST OF FIGURES

CHAPTER 1: INTRODUCTION

1.1 Gas Flaring

Gas flaring is the controlled burning of combustible materials such as hydrocarbon (HC) and H_2S in oil & gas and petrochemical industries during exploration, transportation or processing [1]. During process operation, flaring safely manages the disposal of routine small volumes of unrecoverable waste gas. On the other hand, potential causes for flaring arise during abnormal process upsets such as process equipment malfunction, off-spec production and startups or emergency planed shutdowns [1-3].

1.2 Flaring Adverse Impacts & Global Efforts

According to world bank statistics 149 billion cubic meters (bcm) of associated gas was flared at oil production sites worldwide in 2016 which released millions of tons of CO_2 to atmosphere [4]. Gas flaring has adverse economic, environmental and societal impacts. Flaring of associated gases results in waste of valuable energy source. Environmentally, gas flaring emissions are considered a major contributor to global warming. Hence, flaring is a major contributor to increasing levels of greenhouse gas (GHG) emissions that impact rising sea levels and altering weather patterns. [2]. Furthermore, GHG and pollutants emissions negatively affects human health. These gases include VOCs, particulate soot and other pollutants which are linked to cause cancers, asthma, chronic bronchitis, blood disorders, and other diseases [5].

Several international regulatory authorities, government organizations and oil companies have initiated and implemented efforts towards emissions reduction [6] such as the

adoption of Koyoto Protocol agreement which obliges its signatories to set emission reduction targets [7], the Intergovernmental Panel on Climate Change (IPCC) which assess the climate change related science globally and help governments to develop relevant policies [8], Global Gas Flaring Reduction Partnership (GGFR), a World Bank-led organization which sponsor the "Zero Routine Flaring by 2030" initiative [9] and Paris Agreement which aims to limit global temperature rise to below 2 degrees Celsius within this century [10]. The state of Qatar is a signatory member of Koyoto protocol [11], GGFR [12] and Paris Agreement [13]. Therefore, the Qatari Ministry of Environment & Municipality initiatives and regulations target to cap Qatar's gas flare to 1% of the inlet raw gas [14] and 0.3% of treated sweet gas among all gas production facilities [15] which is also in line with Qatar's 2030 vision.

1.3 Motivation and Project Objectives

In many countries, flare gas recovery projects are inevitable due to its project CAPEX, limited funding and/or energy subsidies. Utilizing flared gas in existing facility while meeting process safety, energy requirements will result in significant process power savings and GHG reduction with lower initial cost [16]. One of the proposed flare utilizing techniques is to recycle hydrocarbon (HC) rich gas streams to combustion units such as furnaces, boilers and cogeneration units, to utilize their energy content. Fig.1 depicts a processing facility and its cogeneration unit used for supplying heat and power. Streams A-G represent the potential flared gas streams from a process. Fig. 2 presents the proposed process alternative where we are considering the recycle of flared gas

streams to be used as fuel feed to a cracking furnace in the process. For this study, an ethylene process is considered as the base case process.

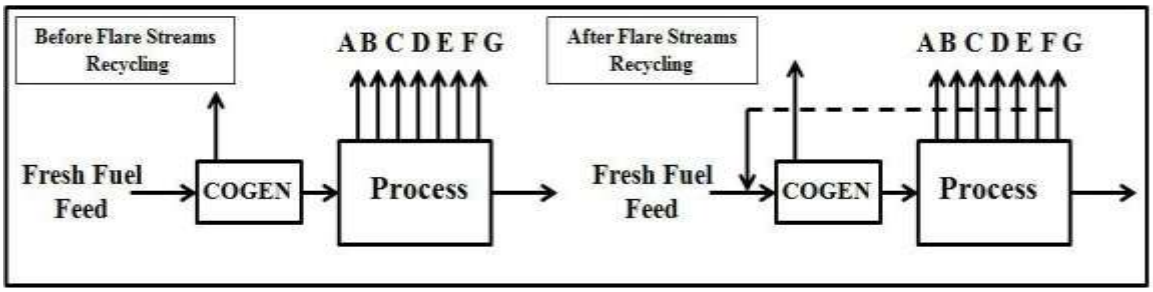

Figure 1.Utilizing flared gas in a pre-sized cogeneration unit[2]

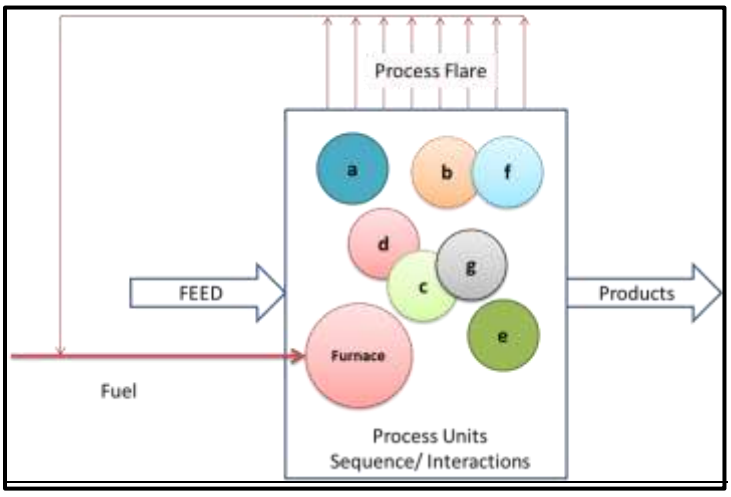

Figure 2.Utilizing flared gas in a cracking furnace

Tim Gandler, energy coordinator in Baytown Olefins Plant, reported that Ethylene cracking furnaces account for 60% of plants energy use as shown in Fig.3 [17]. Hence, we will study the potential to utilize HC flared gas stream in the ethylene process as a fuel feed to the steam cracking furnace.

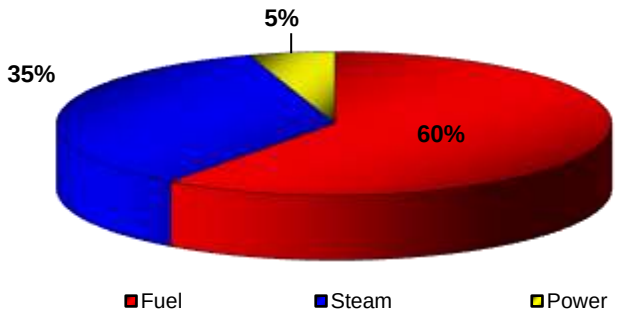

Figure 3.Ethylene plant energy consumption [17]

Compared to other combustion demand units (e.g. gas turbines, boilers, etc.), furnaces offer an advantage when it comes to utilizing HC flared gas as fuel due to its low restrictions regarding fuel composition. Hence, it can combust a wide range of HC gas composition [18] with wide wobbe index range. Furthermore, furnaces operate at higher fuel consumption rate compared to boilers and cogeneration units; and providing larger opportunities for flare utilization. Yet, there is a need to study the impact of recycling "flare streams" as fuel for furnaces with varying composition and at varying flowrate on

the furnace performance. Parameters such as temperature profile from the flare tip, fuel composition, excess air percentage and primary to secondary fuel mass flow ratio are key parameters that greatly impact the performance of the furnace in its ability to crack feed gas.

Hence, the work presented here investigates the influence of composition and WI of flare gas streams as fuel source to ethylene furnace cracker.

1.4 Problem Statement

It is desired to study the technical and environmental impact of recycling potential flare streams on the flue gas side of the furnace. A pre designed ethylene process is used as base case design. Available are:

- Process design and operational data during abnormal operations for an ethylene process. This includes historical flaring upset data: flare stream routes, causes, and duration.
- Flare streams, flowrates and their compositions that are available for recycle based on previous work presented by Kazi et al. [2]. The data is summarize in section 3.2.1.

To address this objective(s), the following tasks will be carried out:

- Search the literature and gather data on furnace and burner geometry for a typical ethylene cracking furnace.
- Construct a 3D CAD model for furnace and burner using suitable software such as Solid Works

- Develop a CFD simulation model for furnace and burner using suitable software such as ANSYS Fluent
- Validate the stability of developed CFD models
- Conduct a temperature profile analysis to investigating the effect and limits of utilizing flare streams as fuel source on the flue gas side of the furnace.
- Asses the suitability and impact of varying fuel feed flowrate and composition on the burner combustion and furnace performance.
- Assess the environmental impact of recycling otherwise flared stream on the process

In this wok, Chapter 2: Lecture Review, will brief some common flare reduction techniques followed by an overview industrial fired heaters and burners. Then, CFD modeling and GHG tracking & taxation are discussed. Research Methodologies, Chapter 3, shows the CFD Base case building blocks and the ethylene bases case including its flaring profile followed by in-house developed GHG calculator. Finally, Results & Discussion, Conclusion & Future Work are discussed in Chapters 4 and 5 consequently.

CHAPTER 2: LITERATURE REVIEW

2.1 Flare Minimization Techniques

Current techniques to reduce GHG emissions from flared gas includes

- Injection into oil & gas wells or gas-gathering system by compression [19, 20]
- Converting flared gas to liquefied petroleum gas (LPG), liquefied natural gas (LNG) [20]
- Storage as feed stock for petrochemicals production [20]
- Using as utility feed for onsite steam and power generation through plant fuel network [20, 21]. Kazi et al. developed an optimization framework for sizing a COGEN unit to utilize flared gas from uncertain sources. The results showed that sizing the COGEN is a key factor on capping GHG tax with associated economic loss and environmental impact [21]. Fahd et al. used in house generic GHG gas calculator to assess the GHG impact from proposed COGEN [6].

2.2 Ethylene Process Overview

Ethylene is mainly produced by steam cracking of hydrocarbon feedstock such as naphtha, gasoil and higher hydrocarbons as in Europe and Asia or ethane and propane as in US, Canada and Middle East. The process mainly consists of four major blocks: cracking, quenching, compression and drying, and separation. Fig.4 illustrates the sequence of ethylene production process sections. In the cracking section, hydrocarbon feedstock is cracked at low pressure and high temperatures (600-800 ^{0}C) [22] to ethylene,

lighter products including hydrogen, and other by products. The compression and drying section, raise the pressure of the products to derive the flow along the process and enhance the downstream separation profile. Within compression stages acid gas is being removed through caustic soda tower and water is being separated through driers to prepare for the next separation section at cryogenic temperatures. The separation section consists of multiple distillation columns where ethylene and byproducts are being separated based on their differences in boiling points.

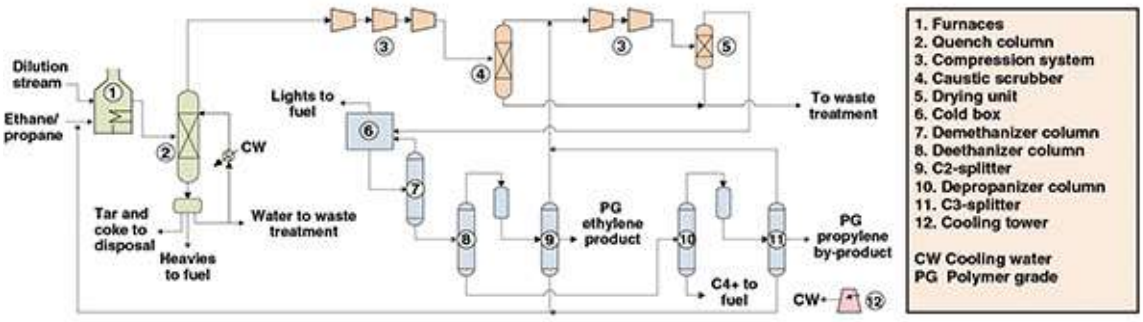

Figure 4.Ethylene process flow diagram [23]

2.3 Fired Heater Characteristics

2.3.1 Fired Heaters

Fired heaters (or Furnaces) are equipment used to heat fluids flowing in inner tubes along the heater where the tubes are heated by means of radiative and convection heat transfer from direct fire fuel burners. Furnaces are commonly used in hydrocarbon, chemical and petrochemical process to heat. Furnaces can be classified to many types according to function, geometry, burner arrangement, draft type, firebox temperature, etc. The most common types of furnaces based on its function are:

Reformers: Used to reformulate a chemical feed stream into another product such as the hydrogen reformer where natural gas feed is being reformulated into hydrogen by endothermic catalytic chemical process [24].

Cracking furnaces: Used to crack large hydrocarbon molecules into smaller molecules such as ethane feed cracking into ethylene and associated by products.

Other types of fired heaters include startup heaters, fired reboilers, process heaters, process heater vaporizers, and crude oil heaters [25]

2.3.2 Fired Heater Geometry

Fig.5 shows a cross section of a natural draft furnace. The geometry from bottom to top is as follows:

Radiant section or firebox: where burners are mounted to heat the radiant coils. Around 85% of the heat release from the burners should be transferred to radiant coils in this section [25].

Shield section: located between radiant and convection section where rows of tubes protect the convection tubes from direct radiant heat [25].

Convection section: where flue gas heat is being utilized to preheat process feed inlet prior to radiant section inlet.

Breaching section and stack: located above convection section where most of emission analyzers and combustion air flow control damper are mounted.

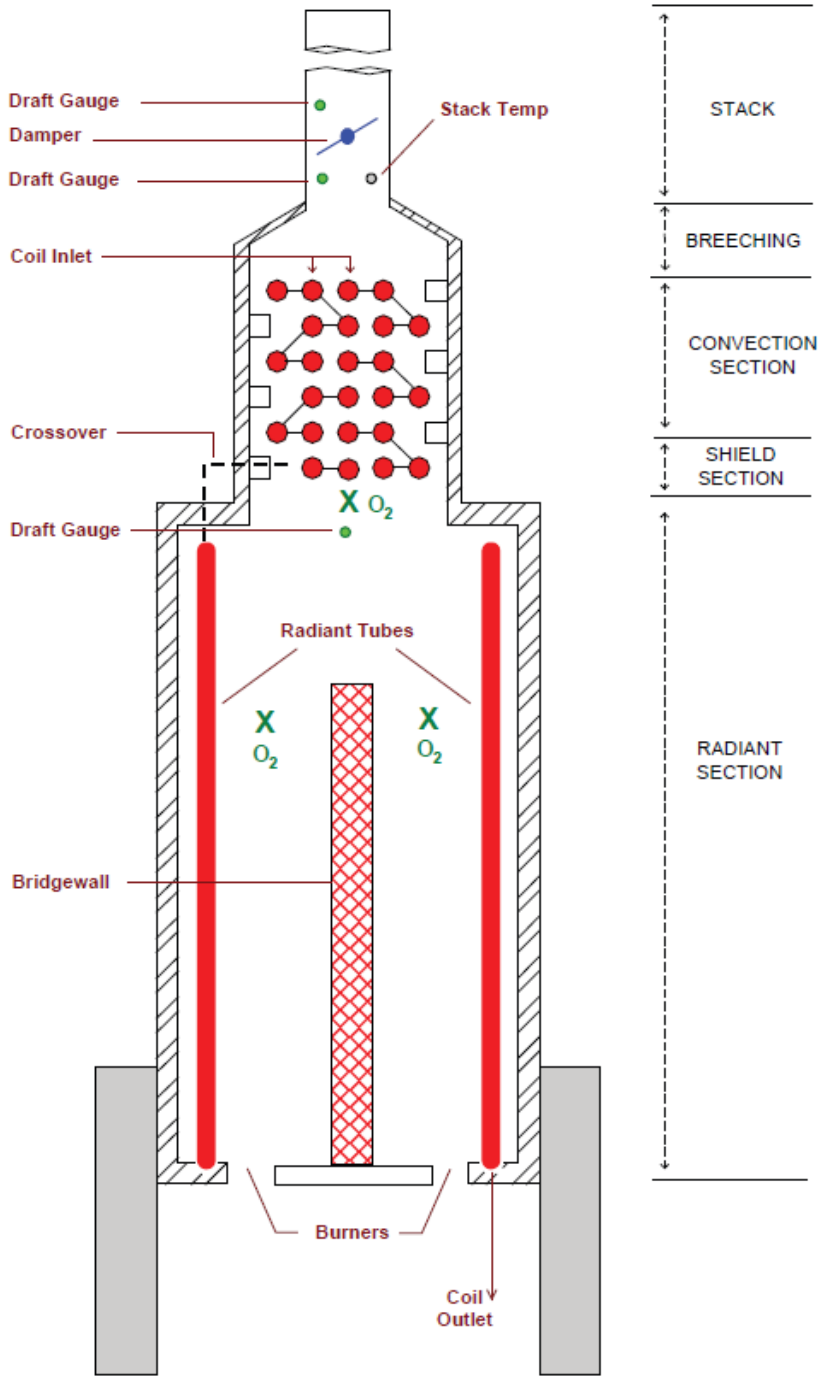

Figure 5.Sections of a process heater [25]

2.3.3 Fire Heaters Duty

Furnaces are high energy demand industrial equipment due to its fuel consumption with a duty ranges from 1.5MW in a small hot oil heater to 440MW of a reformer or a cracking furnace [26]. The mean size of a natural draft heater is 21MW and can go as high as 32MW for a forced draft heater [24]. Table 1 list few of the most common heaters in chemical and hydrocarbon industry classified to fire box temperature. AMETEK Process Instruments, a worldwide analyzer and instrument manufacturer, estimates that energy cost represent 65% of a chemical complex OPEX where furnaces and heaters are the major contributors [25].

Table 1.Major Fired Heater Applications in the Chemical Industry [24]

Chemical	Process	Heater Type	Firebox Temperature (°F)	1985 Fired Heater Energy Requirement, (10^{12} Btu/year)	% of Known Chemical Industry Heater Requirements
Low- and medium-temperature applications					
Benzene	Reformate extraction	Reboiler	700	64.8	9.9
Styrene	Ethylbenzine dehydrogenation	Steam superheater	1500–1600	32.1	4.9
Vinyl chloride monomer	Ethylene dichloride cracking	Cracking furnace	N/A	12.6	1.9
P-xylene	Xylene isomerization	Reactor fired preheater	N/A	13.0	2.0
Dimethyl terephthalate	Reaction of p–xylene and methanol	Preheater, hot oil furnace	480–540	11.1	1.7
Butadiene	Butylene dehydrogenation	Preheater, reboiler	1100	2.6	0.4
Ethanol (synthetic)	Ethylene hydration	Preheater	750	1.3	0.2
Acetone	Various	Hot oil furnace	N/A	0.8	0.1
High-temperature applications					
Ethylene/propylene	Thermal cracking	Pyrolysis furnace	1900–2300	337.9	51.8
Ammonia	Natural gas reforming	Steam hydrocarbon reformer	1500–1600	150.5	23.1
Methanol	Hydrocarbon reforming	Steam hydrocarbon	1000–2000	25.7	4.0
Total known fired heater energy requirement				652.4	100.0

Source: Sanderford, E.B., Alternative control techniques document—NOx emissions from process heaters, U.S. Environmental Protection Agency Report EPA-453/R-93-015, February 1993.

2.4 Burner Characteristics

2.4.1 Industrial Burners

Industrial burners are mechanical devices used to convert a fuel's chemical energy to thermal energy through properly mixing and combustion of the fuel with an oxidizer while maintaining a stable flame inside fired equipment [18, 27]. The type, number, and arrangement of burners within a combustion system are related to application size and type.

2.4.2 Burner Design Considerations

Burner design should sustain acceptable flame pattern at specific operating condition to meet process requirements [28]. Operating conditions are summarized as per American Petroleum Institute (API) standards, and they include [28, 29]:

- Fuel type & composition range
- Fuel heat release range
- Fuel temperature and maximum pressure
- Liquid fuel maximum atomizing medium pressures available
- Oxidant type and temperature
- Draft and flame type
- Furnace dimensions and firebox temperature

The key characteristics of a well-designed burner is it should efficiently guide fuel-oxidant mixture into the flame zone, sustain continuous ignition zone and proper flame

shape while minimizing pollutant emissions [28]. A burner to burner spacing depends on both burner to burner clearance based on flame diameter and burner to tube clearance. Spacing normally ranges between 2-5 ft. [27]. Usually burner is optimized based on fuel selection which is being specified by customer interest as per process specifications.

2.4.3 Burners Capabilities

Burners have the advantage of being able to combust a wide range of fuel composition, even operating with multiple types of fuels one by one or simultaneously [18]. For example, Fig.6 shows a dual-fuel burner capable of combusting gaseous fuel such as natural gas and liquid fuel such as oil. However, operating with different fuel type or composition is challenging from operation point of view. Combustion of different fuels will not result in identical flare pattern (Flame shape, length and diameter) even at the same combustion system [28]. Hence, a systematic approach is required to manage the flame pattern with acceptable pattern tolerance.

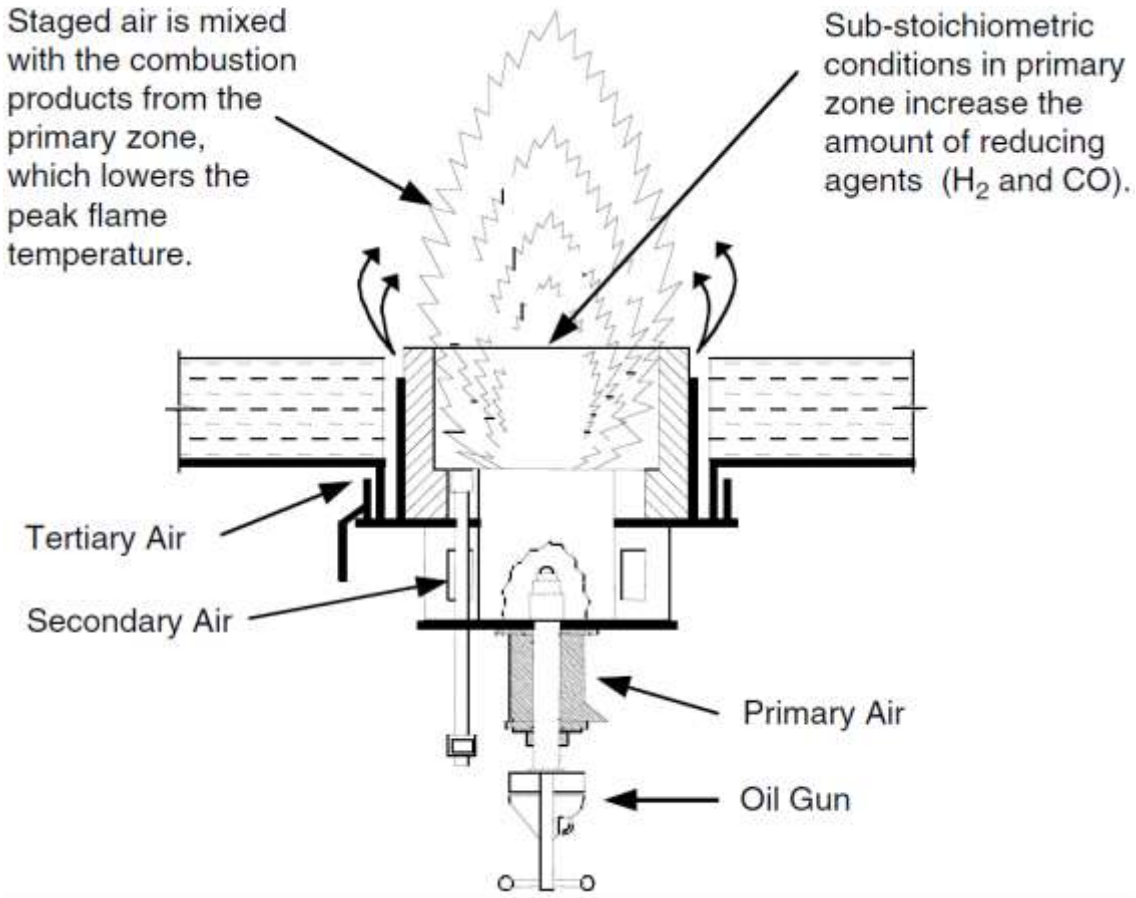

Figure 6.Dual fuel burner (courtesy of John Zink Co.) [18]

2.5 Challenges of Fuel Composition Variance

Test fuel selection, during burner testing phase, is an example of tackling approach. Since customer fuel is difficult to reproduce in testing facilities, a fuel blend is used to simulate customers fuel by reproducing its chemical and transport properties. Table.2 summarizes both chemical and transport properties that are matched to reproduce a closer fuel match. Approximating those properties produces closer burner capacity curves and leads to

combustion with acceptable variance in flame heights, pollutant emissions and flue gas temperature.

Table 2.Chemical and Transport Properties that Needs to be Matched to Reproduce Similar Fuel [30]

Chemical Properties	**Transport properties**
Adiabatic flame temperature	Isentropic coefficient (Specific heats ratio)
Inert content	Molecular weight
Olefins and Hydrogen content	Wobbe Index
Lower Heating Value (LHV)	

The diagram in Fig.7 illustrates the procedure used to approximate a fuel blend to another fuel. In brief the hydrogen, inert and olefins content should be matched or substituted with balanced propylene or natural gas according to rules illustrated in the figure.

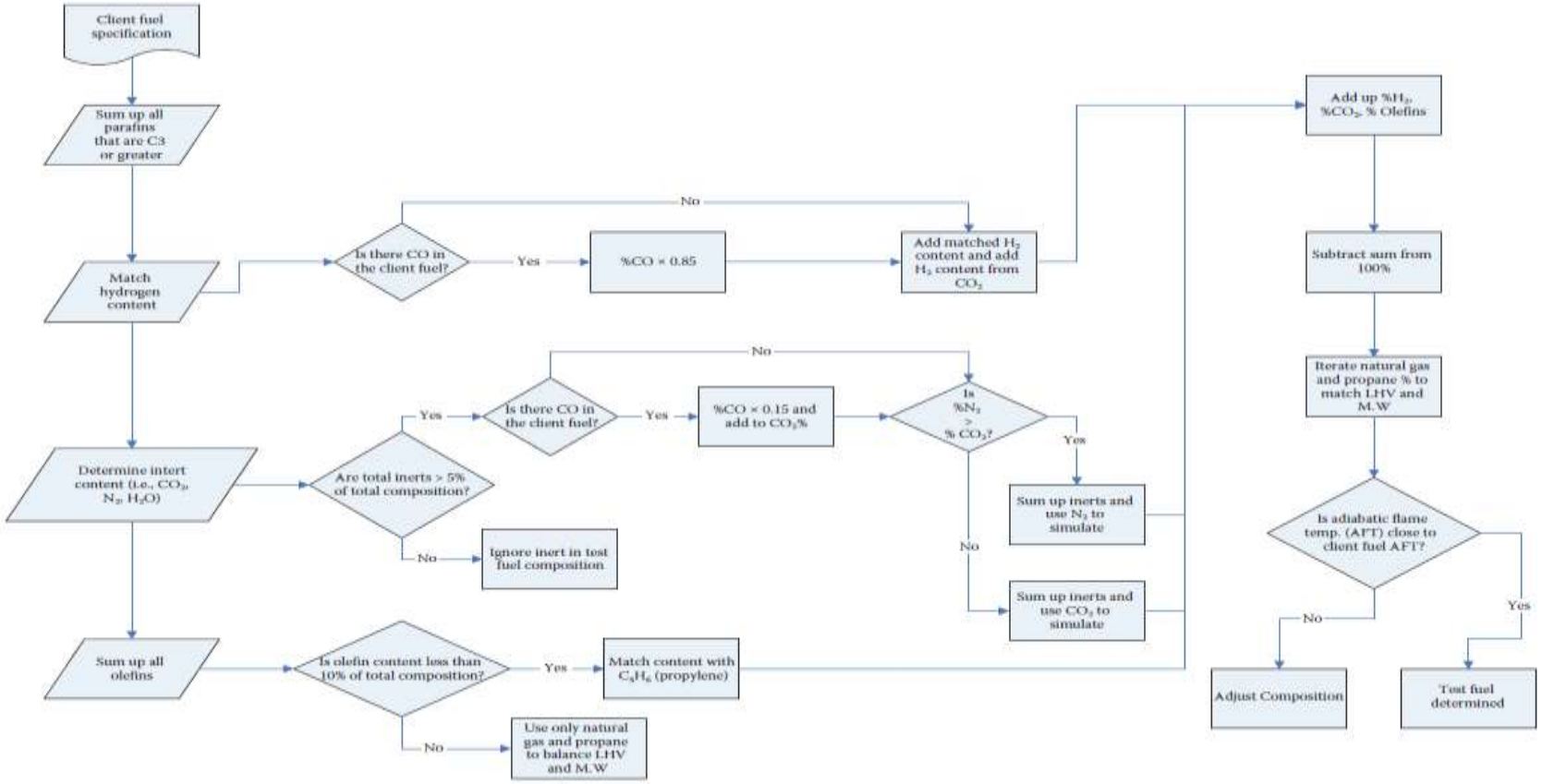

Figure 7.Matching fuel properties process flow diagram [30]

Table.3 and 4 shows a typical refinery fuel gas (RFG) composition and a fuel blend reproduction with close chemical and transport properties based on aforementioned flow chart rules [30]. The hydrogen content was matched. Propylene used to match ethylene content. Natural gas/propane mixture used to match methane and ethane content. Then, the Natural gas and Propylene composition adjusted iteratively to approximate RFG LHV, MW, and adiabatic flame temperature.

Table 3.Example of a Refinery Fuel Gas Composition [30]

Fuel Component	Formula	Volume%
Methane	CH_4	8.13[a]
Ethane	C_2H_6	19.9[a]
Propane	C_3H_8	0.30
Butane	C_4H_{10}	0.06
Ethylene	C_2H_4	32.0[b]
Propylene	C_3H_6	0.78
Butylene	C_4H_8	0.66
1-Pentene	C_5H_{10}	0.07
Benzene	C_6H_6	0.12
Carbon monoxide	CO	0.22
Hydrogen	H_2	37.8[c]

[a] Balance of fuel is primarily methane and ethane.
[b] Level of olefins in the fuel.
[c] Hydrogen content.

Table 4.Fuel Blend Reproduction [30]

Component	Yi (vol %)	Why added	Iterations
Hydrogen	38	To match RGF hydrogen content	N/A
Propylene	28	To match ethylene content	Both compositions where adjusted iteratively to match RFG LHV, MW, and adiabatic flame temperature
Natural gas	34	To match methane and ethane content	

Table 5.Comparison of RFG And Simulated Test Fuel [30]

Property	Refinery Fuel	Test Fuel
LHV (Btu/scf)	1031	1026
HHV (Btu/scf)	1124	1121
Molecular weight	18.09	18.38
Specific heat ratio at 60°F	1.27	1.26
Adiabatic flame temperature (°F)	3481	3452
Wobbe index	1422	1407

2.6 Flame Key Properties

Flame properties varry with fuel composition, direction and distribution of the fuel in the air stream, and port velocity[28]. Few key flame properties are:

2.6.1 Adiabatic Flame Temperature (AFT)

Adiabatic flame temperature (AFT): AFT study is of *interest* due to its influence on heat transfer rate.

2.6.1.1 AFT vs equivalence ratio

Maximum AFT is at stoichiometric combustion (equivalence ratio of 1) where there is just enough oxidizer to combust all the fuel stream. Any excess oxidizer will partially absorb flame sensible energy resulting in lower AFT. Fig.8 illustrates AFT vs equivalence ratio relationship where air and fuel are at ambient temperature and pressure (ATP).

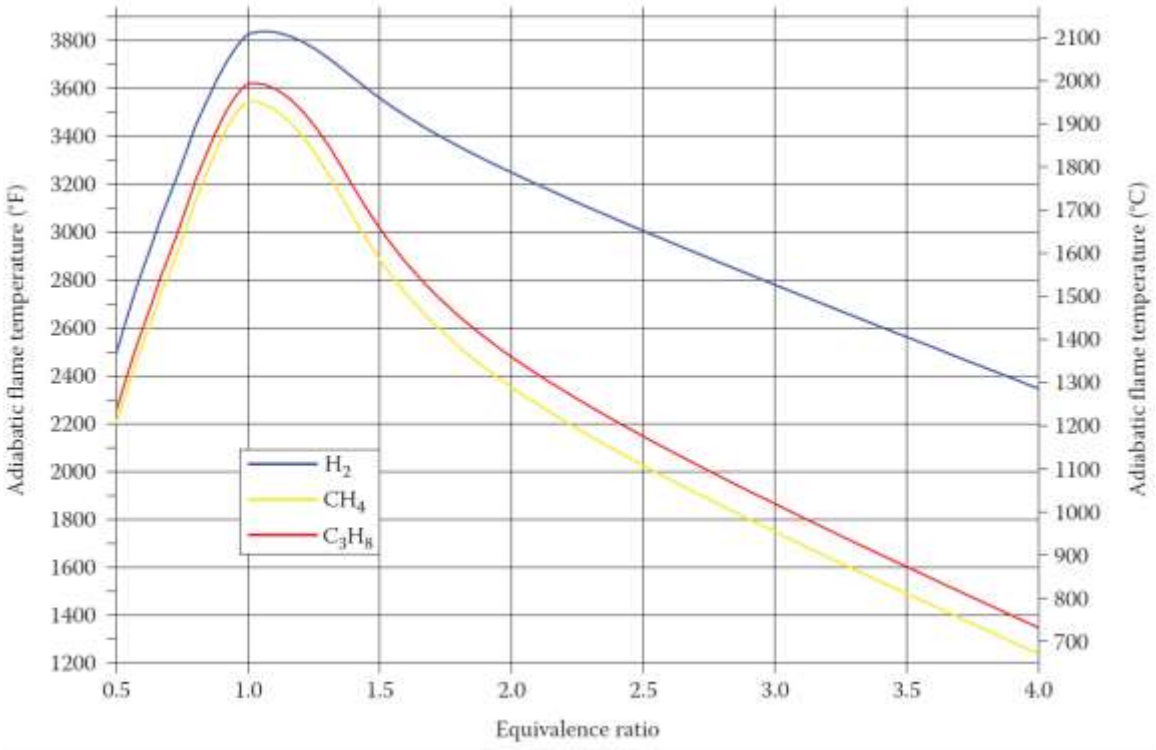

Figure 8.AFT vs equivalence ratio for air/H2, air/CH4, and air/C3H8 flames where the air and fuel are at ATP [31]

2.6.1.2 AFT vs air and fuel preheats

AFT also depends on both air and fuel preheats as shown in Fig.9 & 10. Air preheat has higher effect on AFT increment due to a higher air mass flow rate compared to fuel in a compulsion system. Conversely, preheating air consumes more energy. Fig.11 shows another example of fuel preheats for methane hydrogen fuel blend with more obvious nonlinear relation compared to single component fuel in Fig.10.

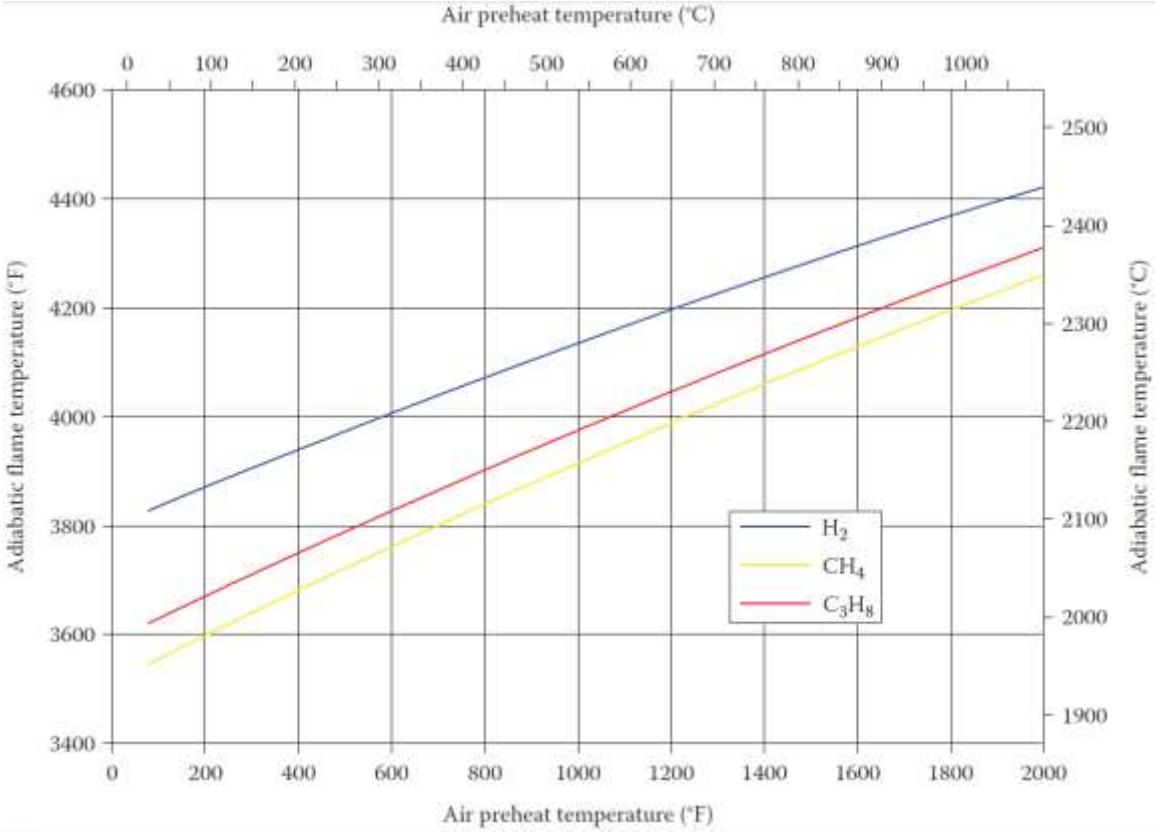

Figure 9.AFT Vs air preheat temperature for stoichiometric air/H2, air/CH4, and air/C3H8 flames where the fuel is at ATP [31]

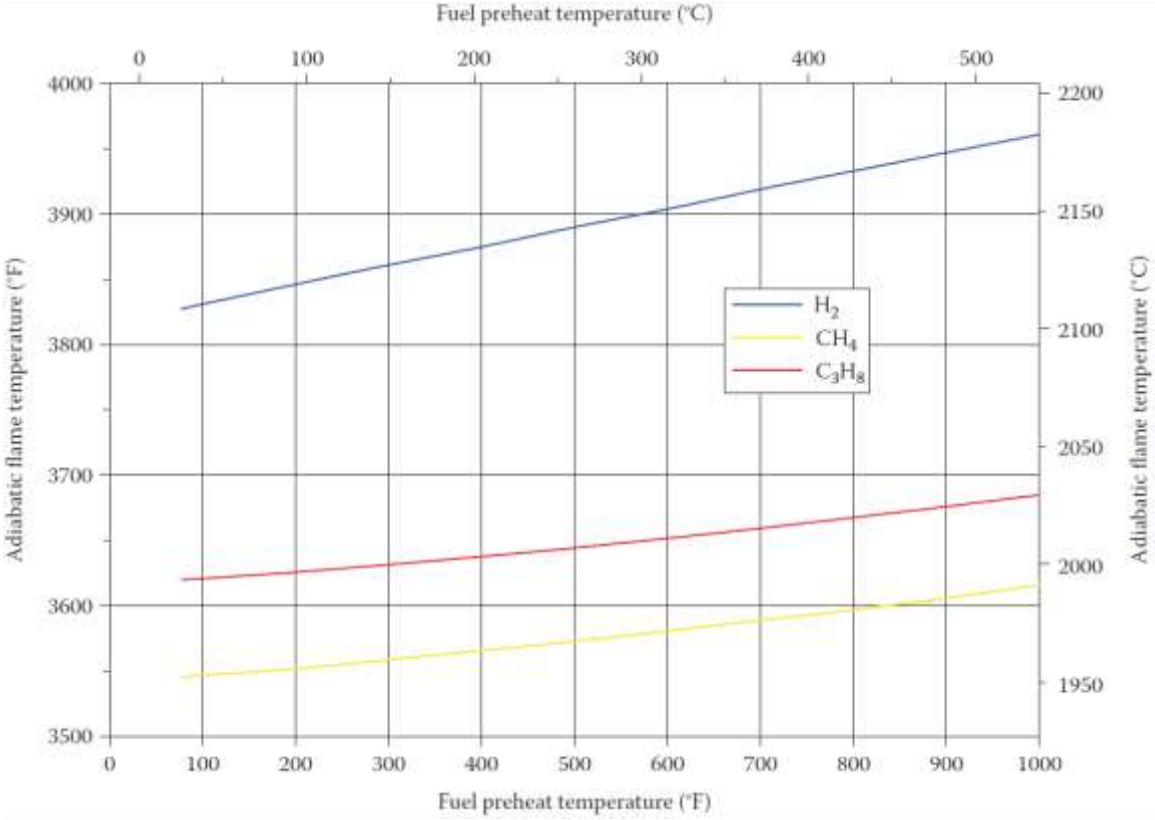

Figure 10.AFT vs fuel preheat temperature for stoichiometric air/H2, air/CH4, and air/C3H8 flames where the air is at ATP [31]

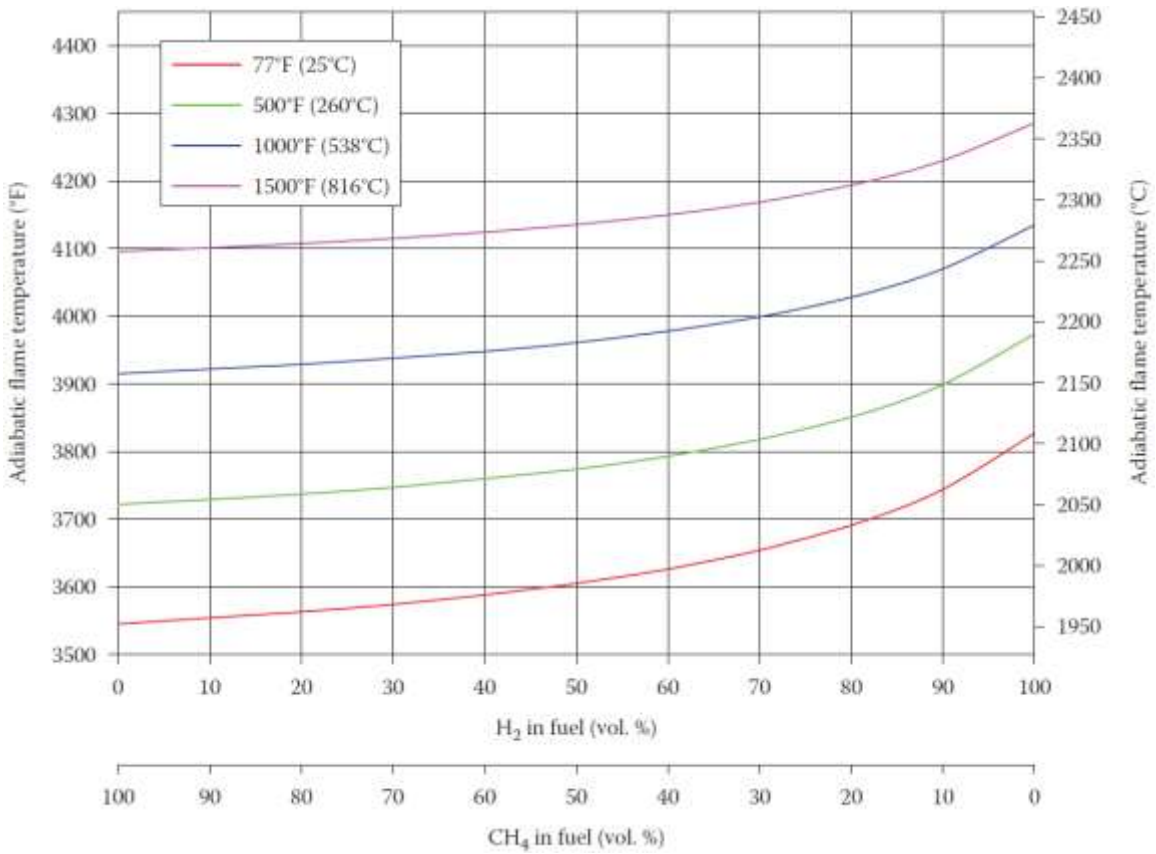

Figure 11.AFT vs fuel blend (CH4/H2) composition and air preheat temperature for stoichiometric air/fuel flames where the fuel is at ATP [31]

2.6.1.3 AFT vs Hydrogen & Nitrogen content

AFT increases with fuel hydrogen content in a nonlinear relation where AFT rapidly increase at high hydrogen content. The opposite for nitrogen fuel content, AFT decreases with fuel nitrogen in a nonlinear relation where AFT rapidly decreases at low nitrogen content. Fig.12 shows AFT for both components.

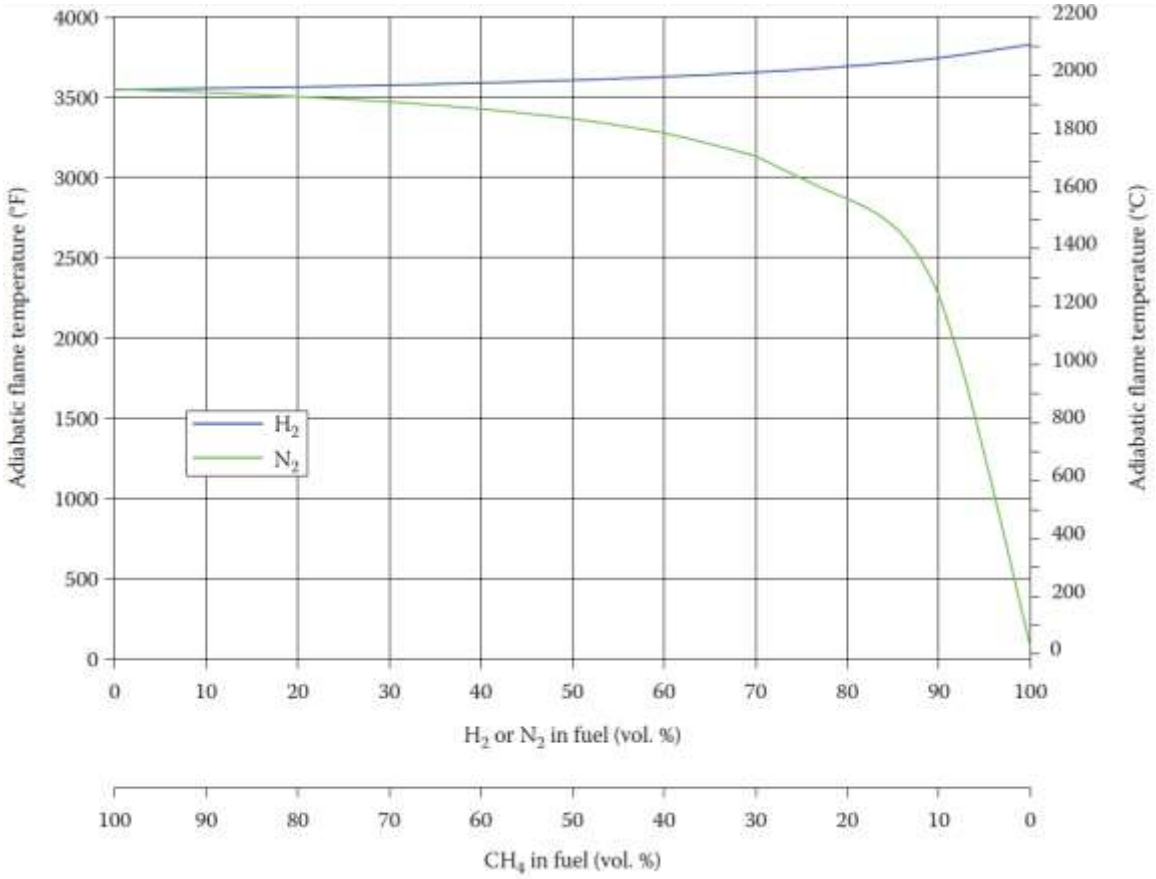

Figure 12.AFT vs fuel blend (CH4/H2 and CH4/N2) composition for stoichiometric air/fuel flames where the air and fuel are at ATP [31]

2.6.2 Available Heat

Available heat is the net heat transferred to the process fluid which is equivalent to the total heat supplied by the fuel combustion excluding energy carried by flue gas, furnace losses by radiations and convection thru furnace walls, and oxidant impurities. Fig.13, 14 and 15 show the available heat as a function of flue gas temperature, air preheat

temperature and fuel preheat temperature. In Fig.13, a higher the flue gas temperature indicates a lower heat transferred to the load. In Fig.14 and 15 the preheat temperature increase indicates a lower available heat to be transferred to the load as the difference was transferred to raise the air or fuel temperature.

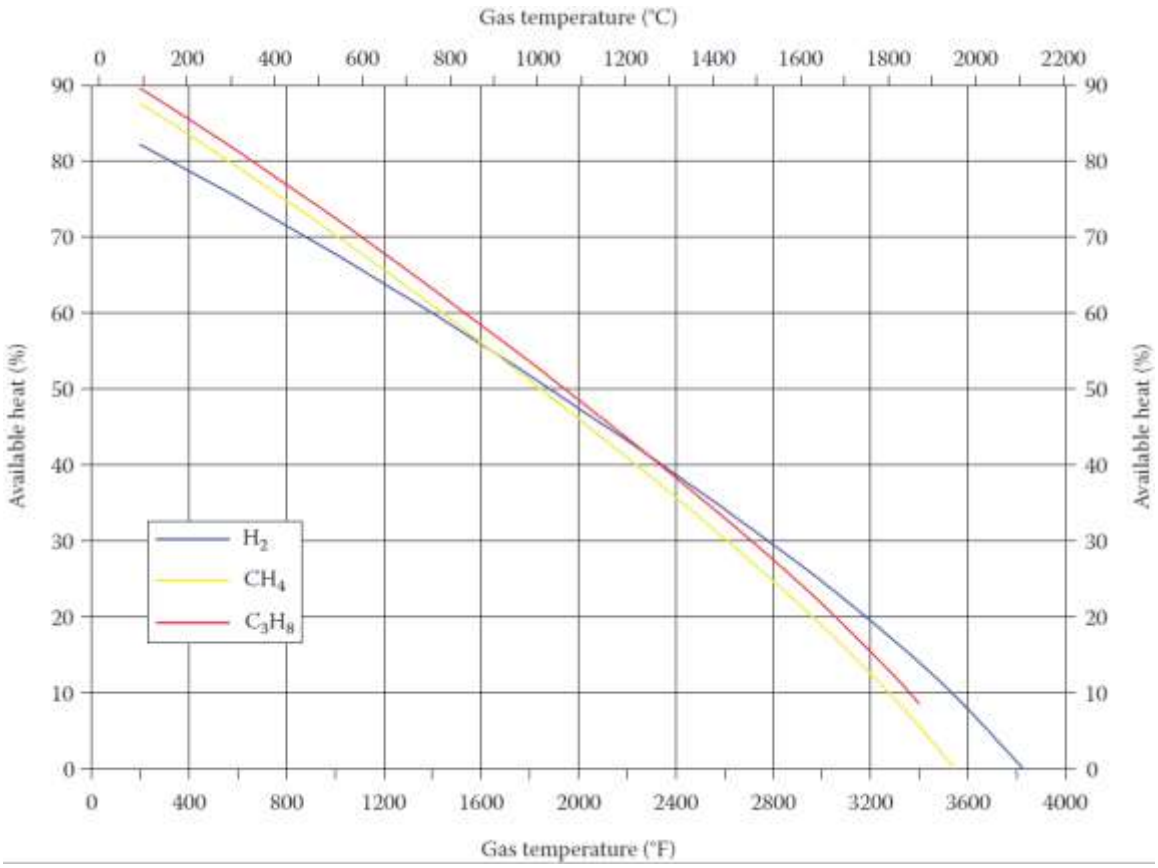

Figure 13.Available heat vs gas temperature for stoichiometric air/H2, air/CH4, and air/C3H8 flames where the air and fuel are at ATP [31]

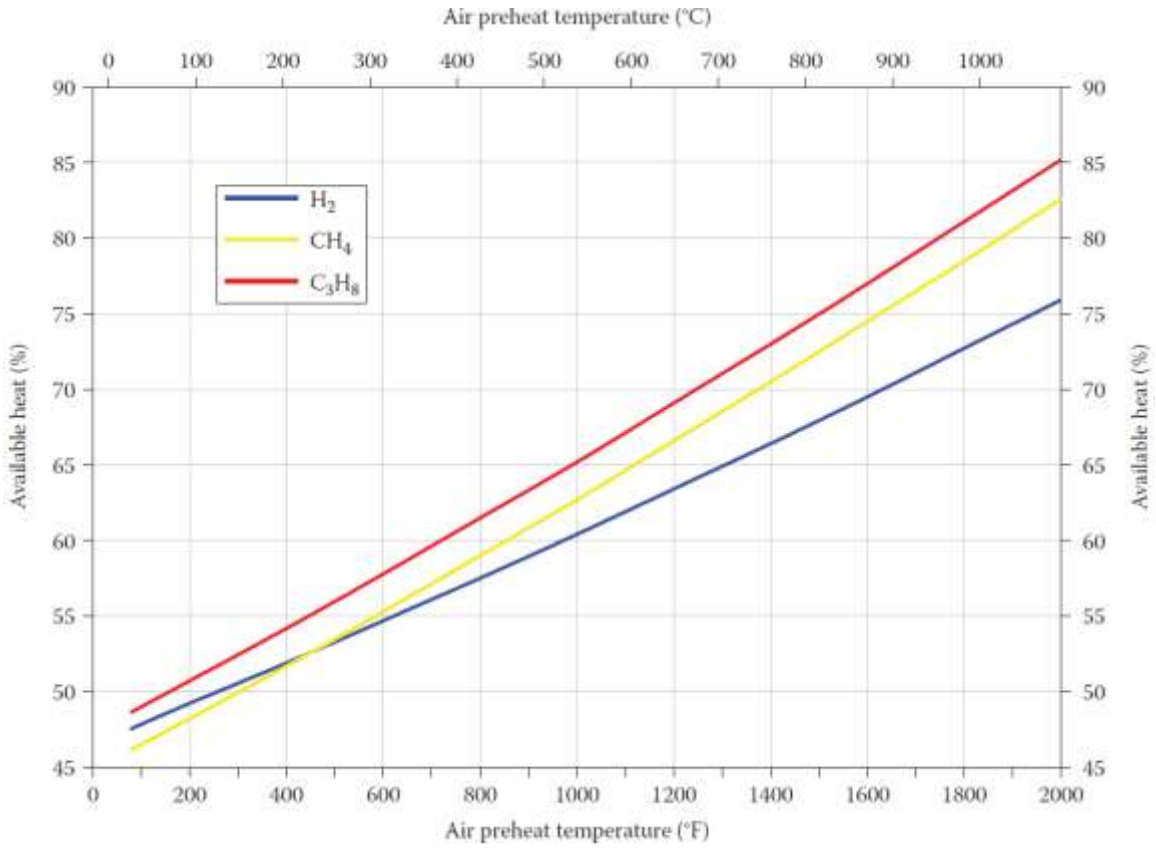

Figure 14.Available heat vs air preheat temperature for stoichiometric air/H2, air/CH4, and air/C3H8 flames at an exhaust gas temperature of 2000°F (1100°C) where the fuel is at ATP [31]

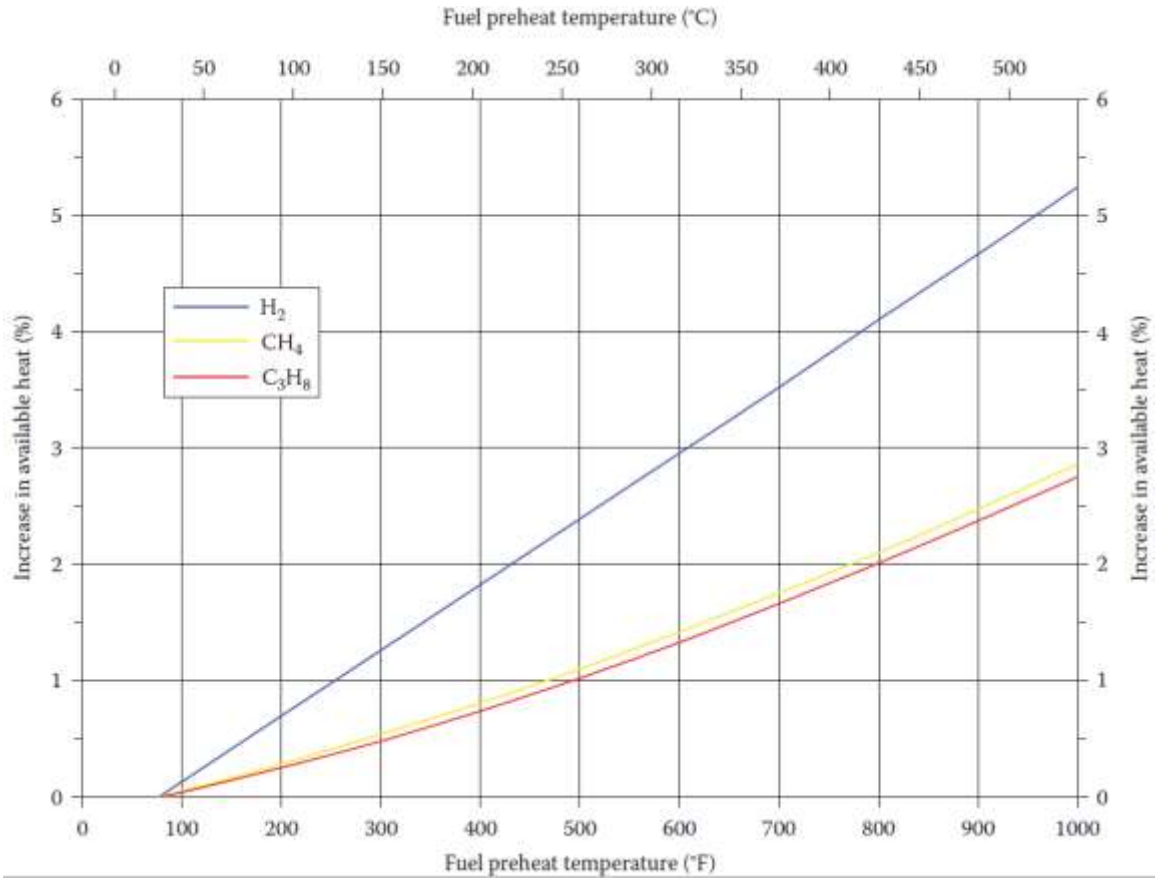

Figure 15.Available heat vs fuel preheat temperature for stoichiometric air/H2, air/CH4, and air/C3H8 flames at an exhaust gas temperature of 2000°F (1100°C) where the air is at ATP [31]

2.7 Computational Fluid Dynamics Simulation

Computational Fluid Dynamics (CFD) is an important tool in aerodynamics and combustion analysis. To construct a CFD simulation, one may need to:

- Understand the physics of the problem
- Formulate mathematical relations that describes the physics
- Use numerical methods to solve governing nonlinear mathematical relations

Then, to build a CFD model, domain, mesh and boundary conditions must be identified.

2.7.1 Domain

CFD domain is the flow domain of the system built as CAD model. Bigger the domain, the higher computational power and time required to solve system governing equations. In furnaces CFD, it is common to simulate a cross-sectional sector of furnace depending on the symmetrical nature of the furnace and burners. However, for that cross-sectional sector, the burner domain must capture all governing physics of burner fuel jets to predict flame pattern within the furnace sector [32]. Experience help compromises between the level of detailed required and computer resources.

2.7.2 Mesh

Solving a system governing equations analytically is not usually practical due to the complexity and nonlinearity between system parameters [32]. Hence, need to divide the domain volume to smaller subdomains to solve discretize differential equations. The small subdomains are called cells while their heads are called grid points and all together

they represent the mesh.

The grid points or so called mesh density differs from one region to another on the overall domain. The mesh density is higher around the areas of interest to capture the related physics such as boundary layer, reaction zone and circulation zone in a burner CFD. Both mesh size and shape impact the accuracy and stability of the CFD solution.

2.7.3 Boundary Conditions

To start CFD simulation, the user must define the boundary conditions around the CFD domain. In other words, to define what goes into and out the system in order to solve the governing differential equation that describes the conservation of mass, momentum and energy. For a well-defined system boundary condition should identify:

- Inlet streams: mass flow rate or velocity, composition, pressure, temperature and phase.
- Outlets streams: exit pressure and flux condition for velocity [32]
- Operating conditions: system pressure and thermal properties such as conductivity, wall temperature, material of construction and wall radiation properties [32].

2.7.4 CFD Models

The CFD model relies of the governing equations of mass, momentum and energy. In burner CFD, model is complex in defining physical and chemical properties such as chemistry-turbulence interactions[32]. Appendix A1 shows general governing equations

in burner CFD simulations. The CFD model predicts mean gas properties in 3D dimension's, steady and turbulent flame velocity, temperature, density and composition, particle and droplet size in multiphase reactions [32]. Figure 16 show associated sub models in in simulating burner CFD.

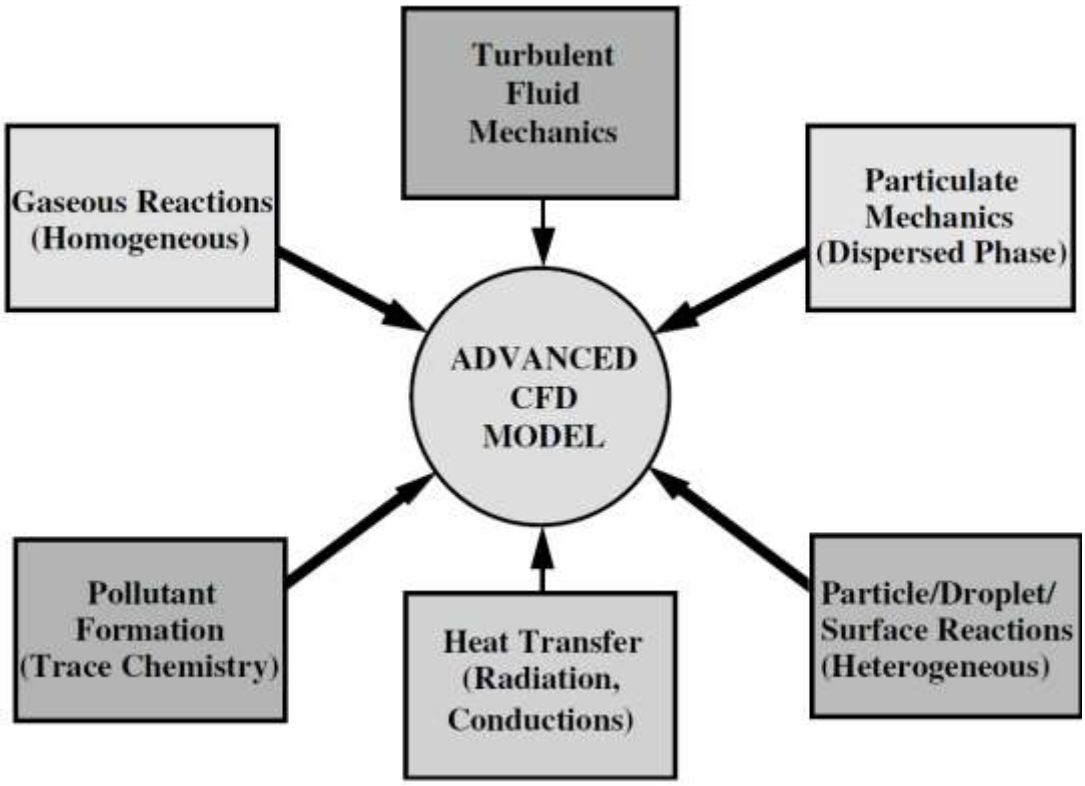

Figure 16.Typical sub-model components in comprehensive CFD code [32]

2.7.5 CFD Strengths and Inabilities

CFD shortened burner development cycle while maximizing its efficiency and lifetime. The tool allowed engineers and scientist to explorer many design and operating parameters in burner design. In addition, allowed for investigating designs which was experimentally impossible due to safety constraints [32]. However, like any tool, CFD have strengths and downfalls in combustion analysis as summarized in Table 7.

Table 6.Strengths and Downfalls of Combustion CFD

Strength	Downfall
• Predicting disastrous failure [33] • Visualizing results and predict non-reactive gaseous flows[33] • Qualitative analysis of temperature, velocity and radiation heat flow[33] • Visualizing flame pattern and geometry shape change effects[33] • Allow to test new operation parameters of existing system[32] • CFD analysis supports planning real experiment and reduce cost of unnecessary real experiments[32] • Prediction of flame interaction in furnaces and associated flame impingement or rollover process tubes	• Limited explanation for complex reactive flow systems specially for complex fuels such reaction kinetics, multiphase reactions, solids reactions and deposition (e.g: soot)[32] • Scientific and cost related difficulties while evaluation real furnaces which can arise from numerical error or experimental data error[32] • Typical CFD tools are not designed to optimize combustion equipment such as burners[32] • Difficulties in predicting premixed fuel combustion[30] • Difficulties in predicting emissions and pollutants due to the variation of reaction rates between main combustion reaction and NOx formation.[30] • Excessive refinement for near burner zone which requires more mesh size, computational power and time subsequently[30]

2.8 GHG Emission Tracking & Taxations

Reporting of GHG emission plays a significant role for industry. Suitable and adaptable GHG tracking methodology is necessary to comply with the regulatory authority's requirements and to explore mitigation approaches for industrial flaring [6, 34]. Global efforts towards GHG emission reduction are being done by policy makers who argued for a long time to impose a price for carbon equivalence emissions due to its environmental and social damage. Worldwide, there are two approaches for tracking carbon pricing. Carbon tax is one of them where tax depends on type of burned fossil fuel and its carbon content. And other is the cap-and-trade (CAT). In the carbon tax approach, the tax is passed on to end users through petrol stations, electricity bills and products cost. Managing carbon tax price is important in many countries such as British Columbia (BC), Canada. For example, BC government started implemented carbon tax in July 2008 at a rate of 10 Canadian dollars per CO_2e metric ton with an annual increment of 5 Canadian dollars till 2012, considering no further increase or planned policy change. Therefore, according to BC's price management guideline, the carbon tax in 2014 was about 30 Canadian dollars, equivalent to 23.03 U.S dollars per metric ton of CO_2e [35, 36]. Table 8 summarizes major pros and cons of Carbon Tax legislation.

Table 7.Pros vs. Cons of Carbon Tax Legislation [37]

Pros	Cons
• Support changing to renewable & clean energy	• Generates regressive effect of taxation
• Revenues can be invested in environment protection	• Increases enterprises' costs
• Lower administrative cost, easier implementation and more predictable effects	• Affects energy price & supply–demand relationship

In the CAT approach, generation companies (GENCOs) hold emission permits. These permits are being distributed or sold through a regulatory agency, and can be traded later on. The overall amount of emissions permits is limited by a pre-determined cap, which will be progressively tightened over time [38]. The emission trading system of the European Union (EU ETS) uses the CAT approach; and it the largest multi-national greenhouse gas emissions trading system in the world [38]. According to the EU Commission GHG reduction strategy in 2009, Europe aim to reduce GHG emissions to 20% by 2020, 40% by 2040 and 80-95% by 2050 compared to 1990 GHG emissions [39]. In fact, EU ETS controls about 50% of EU CO_2 emissions and supports developing a market for carbon permits [40]. Recently, CO_2 average trading price in Europe during April 2016 is about 6.18 Euros, equivalent to 7.01 US dollars per metric ton of CO_2 [41]. The key advantage of CAT legislation is it sets a clear overall emission limits, after

which industry is forced to achieving the overall allowable emissions target with the lowest conceivable cost [42]. Consequently, a key emitter country like Australia is converting from carbon tax to CAT. The Australian senate voted in July 2014 for repealing country's carbon tax and plan for emission trading scheme (ETS) [43]. The ETS has targeted to be the third largest emission trading scheme after Europe and Guangdong, China within 2015 [44].

The estimation of CO_2 emissions, using appropriate emission factors, conversion factors and heating values, is crucial step for building GHG calculator. It is also important to maintain proper documentation of CO_2 emission in order to monitor the approach towards GHG reduction [45]. In this work, a GHG calculator has been developed to estimate GHG emissions from fuel combustion and process upset flaring. This GHG calculator can estimate the emissions for different upset scenarios while each scenario has multiple flare sources. It has the flexibility of estimating the wasted energy content of process flared streams depending on mixture Wobbe index using international accredited standards from the EU commission such as DIN German institute for standardization. In addition, the calculator is able to estimate the carbon tax and credit using the latest carbon tax rates at various focal countries around the globe. These added features of the calculator, make it a useful tool for tracking and reporting GHG emissions and it can be used as a tracking tool to develop suitable alternatives for GHG reduction.

CHAPTER 3: RESEARCH METHODOLOGIES

This work includes here main building blocks. Firs the CFD Base case including the Furnace/Buner geometry, computational mesh building and CFD models. Second, the fired heater based HC process (FHBHCP) which is the ethylene process in our work including the flaring profile, duration and composition. Finally, the in-house developed GHG calculator. Fig.17 shows a simplified flow chart for the work presented below.

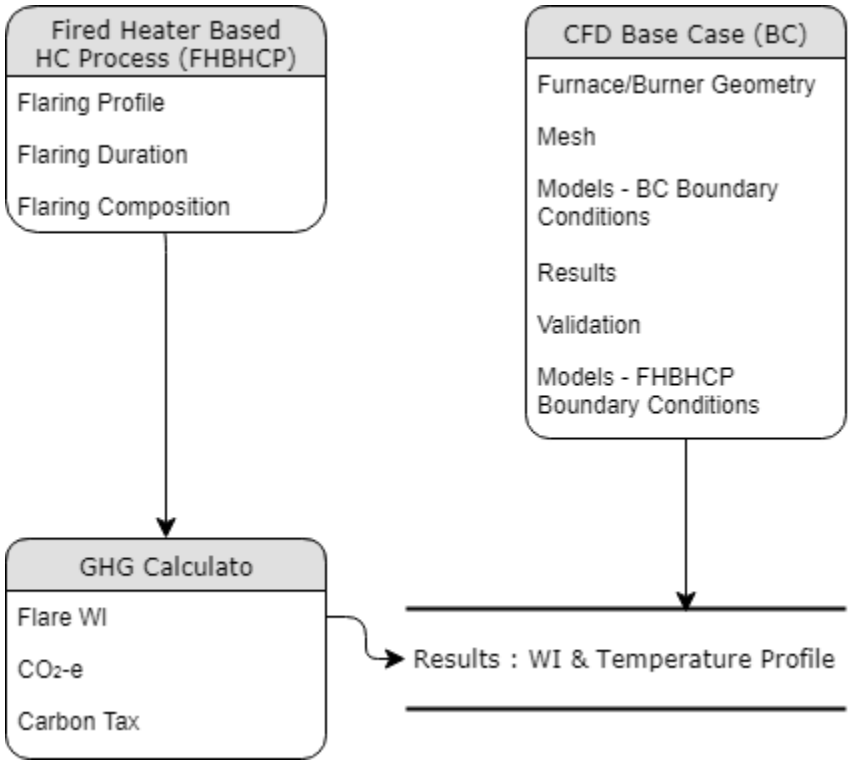

Figure 17. Flow chart of work presented

3.1 CFD Simulation Set Up

3.1.1 Geometry

The geometry of the system depends on Bo Liu's exponential setup. Furnace and burner drown in Solid Works. Outer geometry dimensions are identical while the inner details dimensions were drown from the published reference using a scale factor.

3.1.1.1 Furnace geometry

Furnace is equipped with one fuel-staged low NOx burner (FS-LNB) at the bottom. The furnace sidewalls are insulated with firebreaks. Fig.18 and 19 shows furnace 3D view and dimensions.

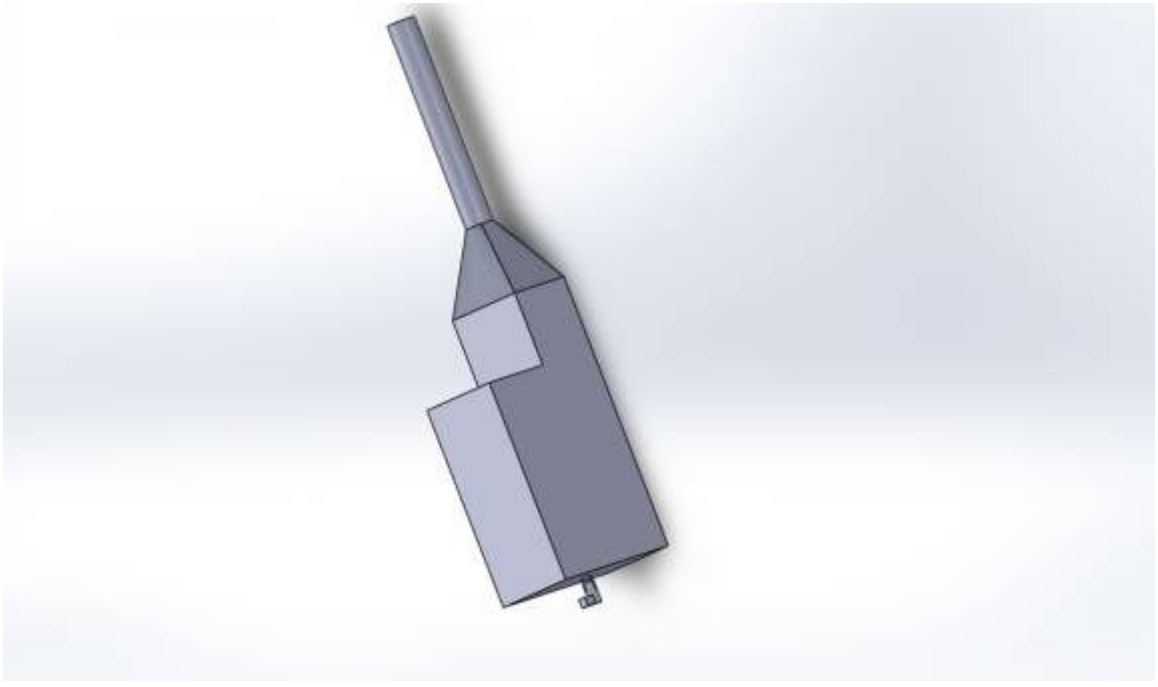

Figure 18. Furnace 3D view

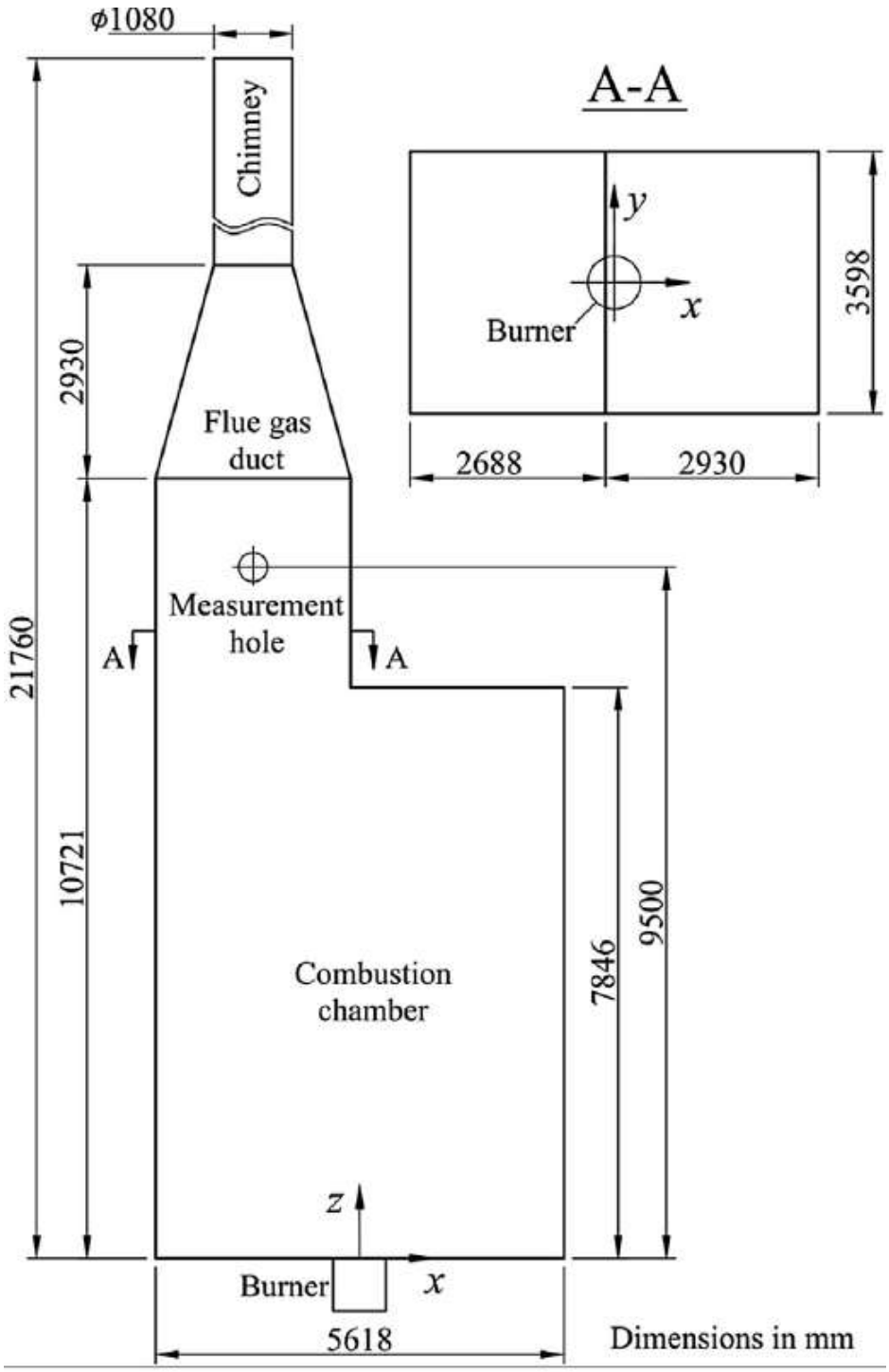

Figure 19.Furnace dimensions [46]

3.1.1.2 Burner geometry

FS-LNB designed to work with tube furnaces. Fig.20 and 21 show burner 3D view and dimensions. The burner consist of

- Air duct
- A venturi shape quarl
- Flame holder to diffuse air flow and create turbulence for initial mixing with primary fuel
- Primary fuel gun with two sets of primary nozzles at different planes. A horizontal set parallel to ground with 4 nozzles each 1.4mm in diameter. An angled set forms a 45 degree with the horizontal plane each 2.8mm in diameter.
- Four fuel staged guns each with three sets of secondary nozzles at different planes. Each gun has a horizontal nozzle, 45 and 75 angled nozzles. Nozzles dimensions are 1.4, 1.5, and 4.6 mm in diameter. The fuel from the four staged guns impinges on the fuel from the primary gun, and then impinges on each other at higher elevation for better air fuel mixing.

The dimensions of flame holder gaps, primary gun elevation from burner base, and secondary fuel guns elevation from burner base were approximated and drown using at scale form printed reference.

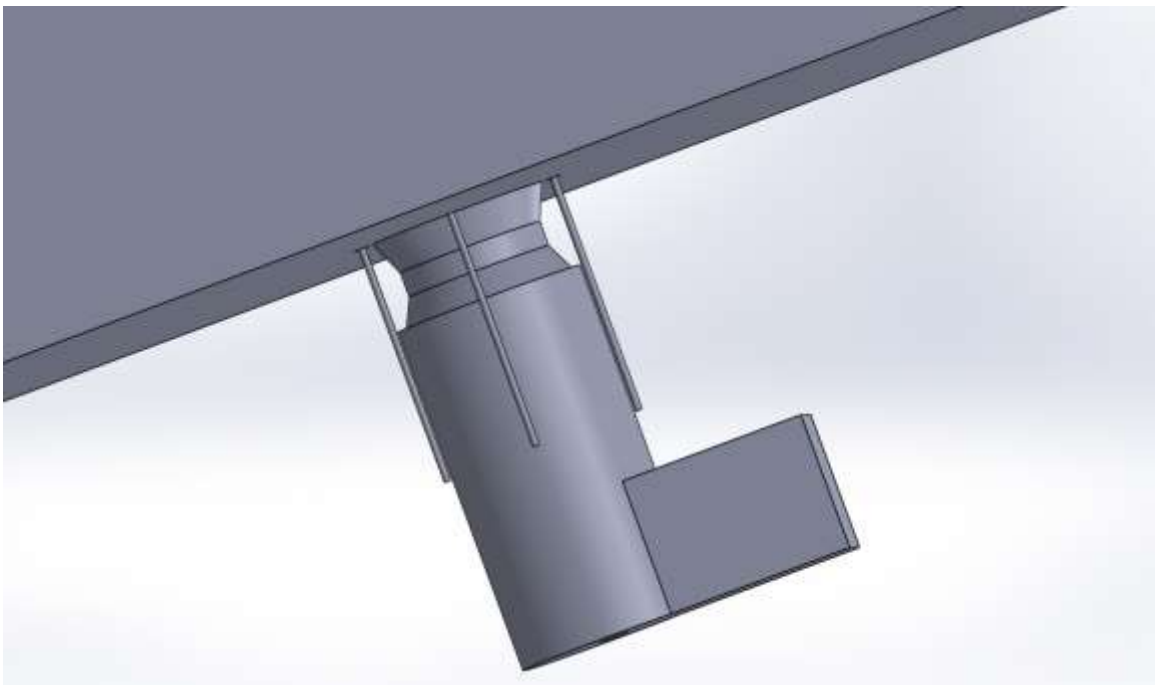

Figure 20.Burner's 3D view

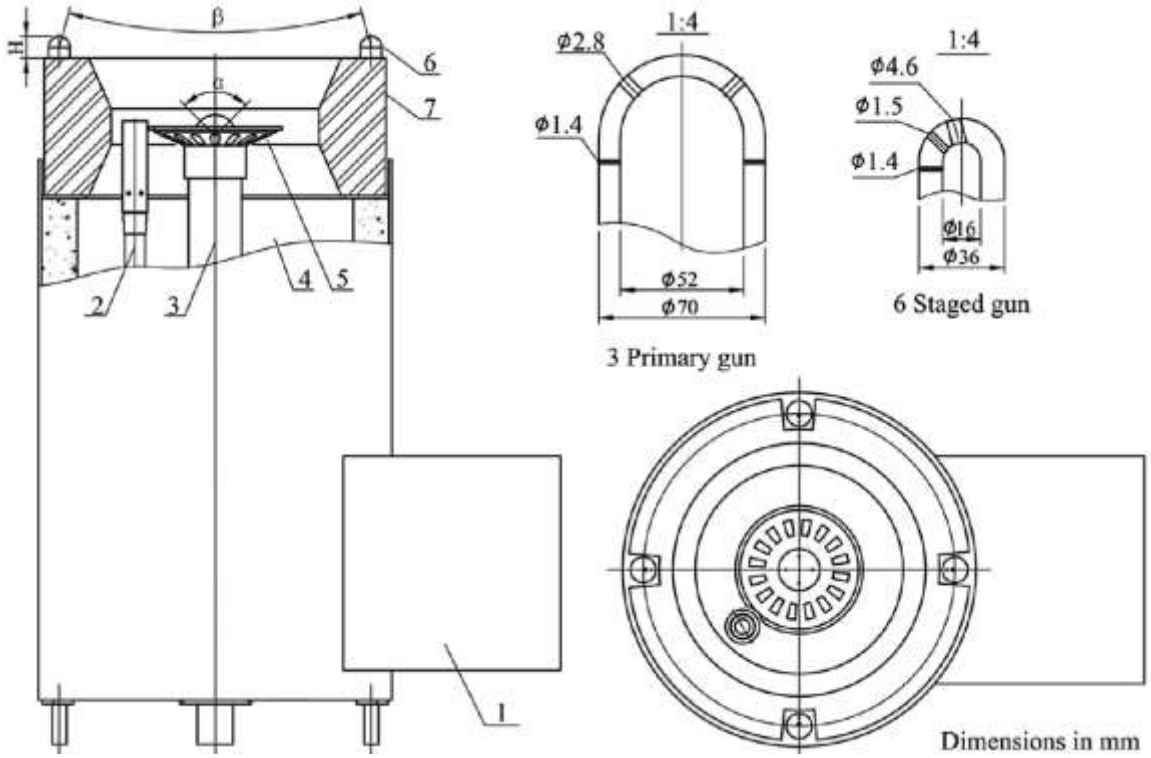

Figure 21.Burner's dimensions [46]

3.1.2 Mesh

The mesh generated using ANSYS Meshing. It consists of around 6 million cells. The mesh density around the burner quarl and fuel guns is the highest as shown in Fig.22 and 23. Fig.24 summarizes mesh sizing properties.

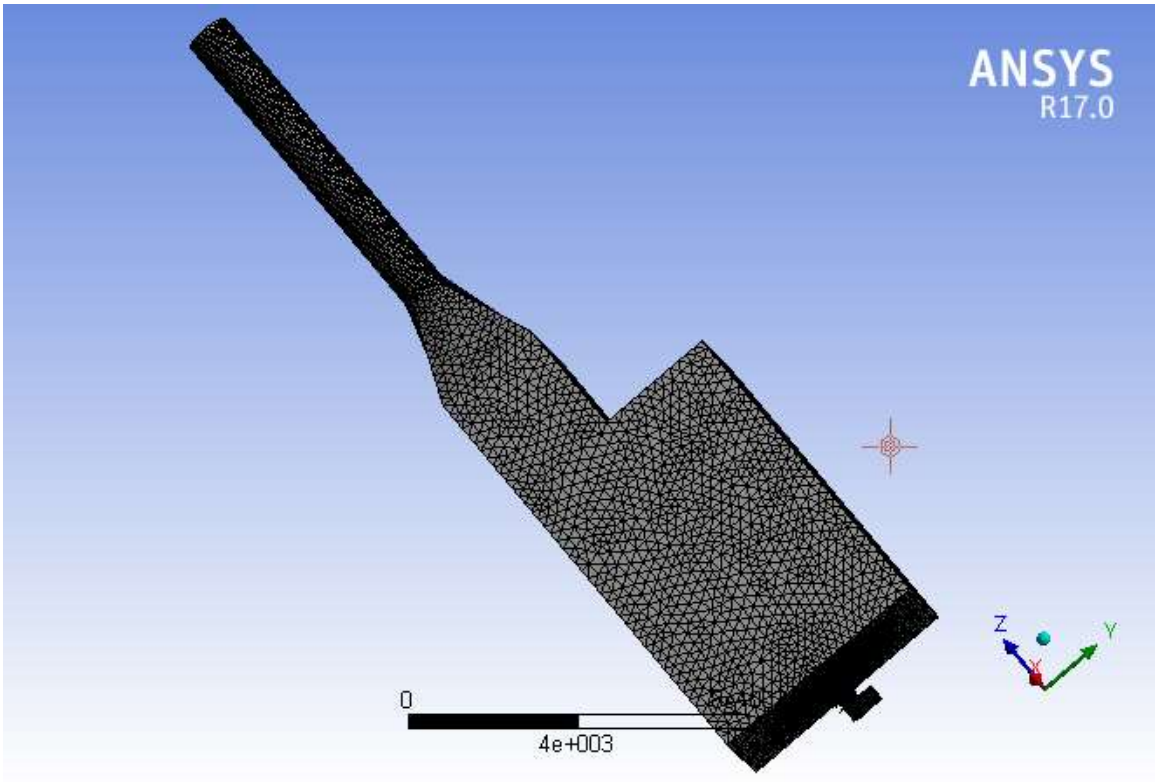

Figure 22.Furnace mesh

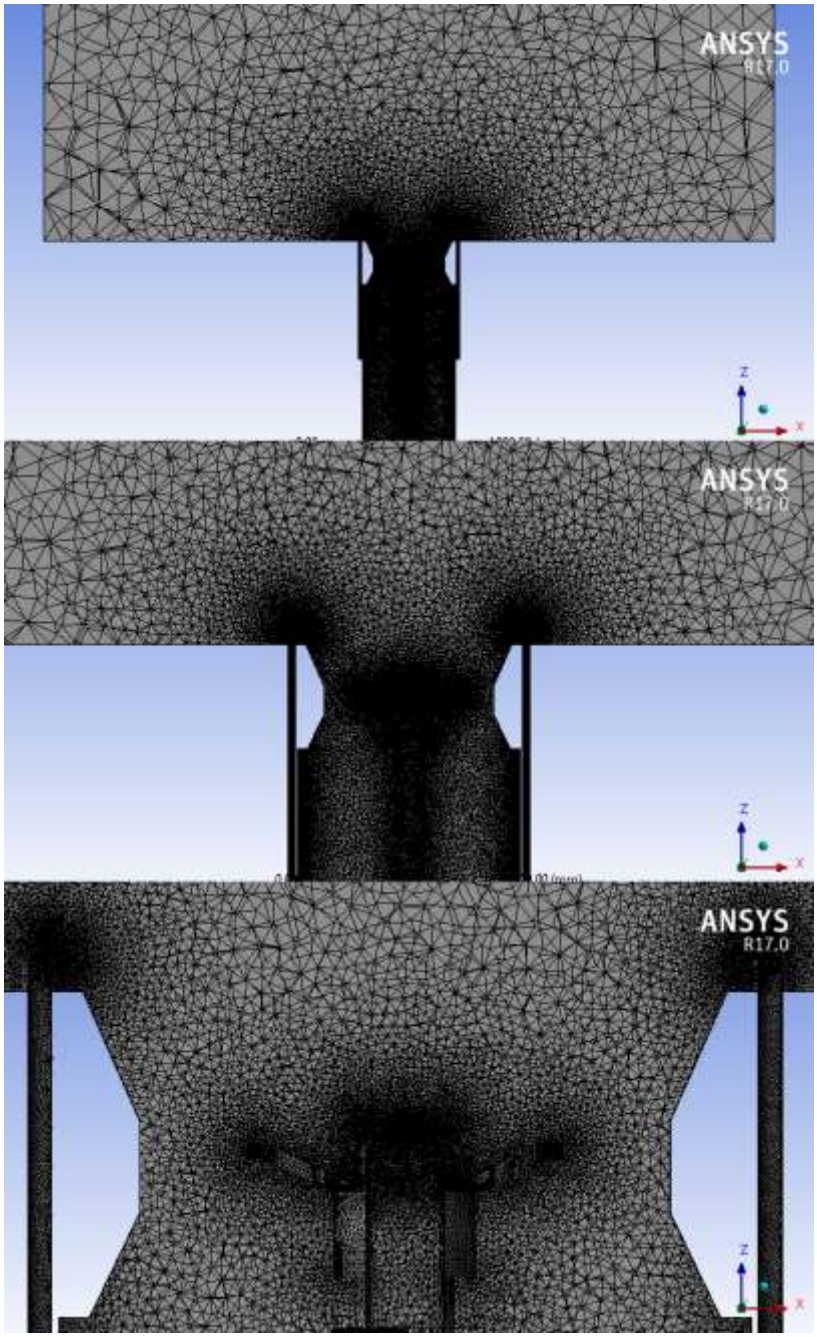

Figure 23.Burner mesh

Details of "Mesh"	
Display	
Display Style	Body Color
Defaults	
Sizing	
Size Function	Proximity and Curvature
Relevance Center	Fine
Initial Size Seed	Active Assembly
Smoothing	High
Transition	Slow
Span Angle Center	Fine
Curvature Normal Angle	Default (12.0 °)
Num Cells Across Gap	Default (5)
Proximity Size Functio...	Faces and Edges
Min Size	Default (2.37760 mm)
Proximity Min Size	Default (2.37760 mm)
Max Face Size	Default (237.760 mm)
Max Tet Size	Default (475.520 mm)
Growth Rate	Default (1.10)
Automatic Mesh Base...	On
Defeaturing Tolerance	Default (1.18880 mm)
Minimum Edge Length	3.23720 mm

Figure 24.Mesh sizing details

The mesh was further refined around primary and secondary fuel nozzles, primary gun, secondary guns, and burner domain using a face sizing of 0.25, 5, 3, and 10 mm element size. Mesh element quality and skewness graphs are shown in Fig.25 and 26.

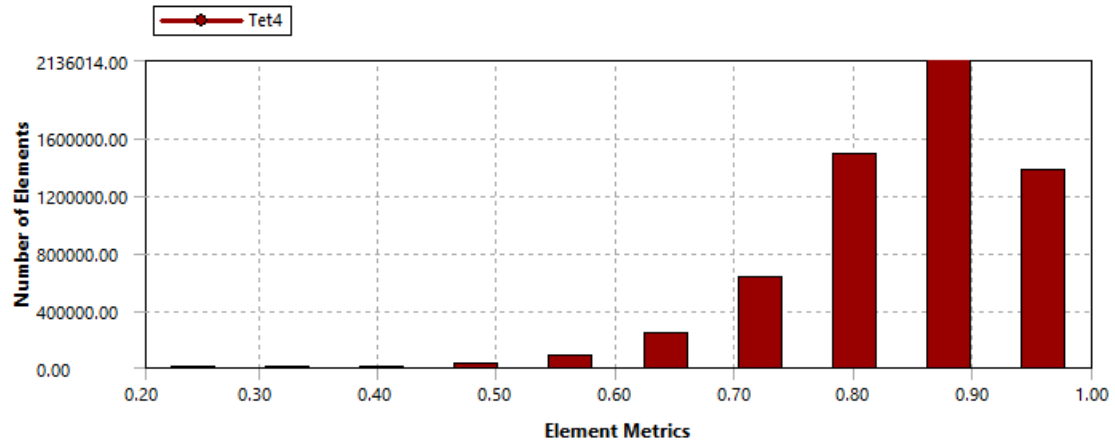

Figure 25.Mesh element quality

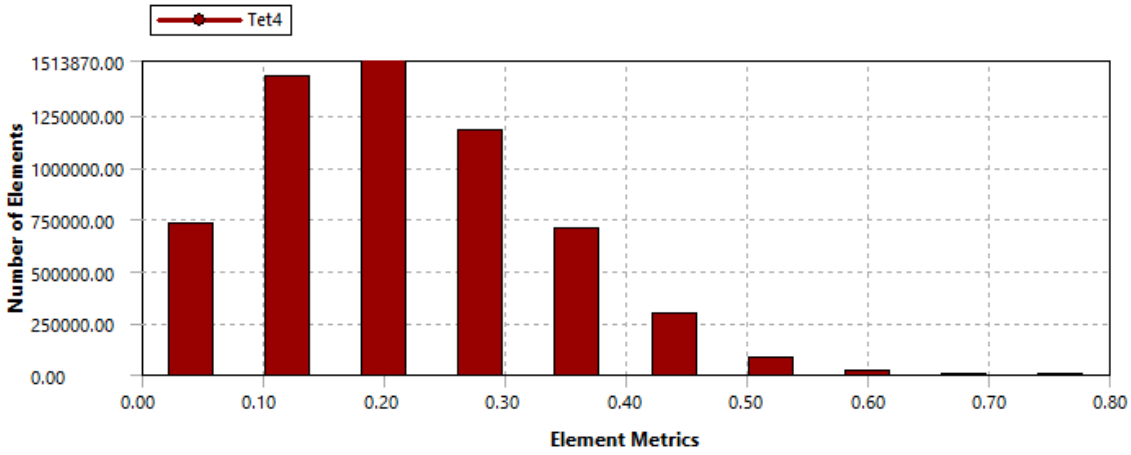

Figure 26.Mesh skewness

3.1.3 Boundary Conditions

The boundary conditions change as subject of study. The boundary condition for the Base Case (BC) model are summarized in Table 11. Furnace bottom wall radiation is - 100 w/m2 and the furnace radiation walls temperature is 1050 K.

Table 8.CFD Boundary Conditions [47]

Boundary	Mass flow rate/(g s^{-1})	Temperature/K	Gauge pressure/kPa	Hydraulic diameter/mm
Primary gas inlet	7.84	300	120	52
Staged gas inlet	20	300	120	16
Air inlet	560	373	0.2	314
Outlet	–	–	0	1080

Based on total fuel and air mass flow rates, the excess air % in the BC model is 18.3%. The excess air percentage will be kept at 18.3% except in experiments studying the effect of excess air % on the temperature profile.

3.1.4 Models

The main equations for solving our CFD model are turbulence and combustion models. Both are described below.

3.1.4.1 Turbulence model

The turbulence flow through the furnace domain is solved through Reynolds-averaged Navier–Stokes equation (RANS) which is a time-averaged equation of motion for fluid flow. RANS is enclosed with standard wall function K-epsilon (k-ε) model account for tangential velocity near the walls [46, 47]. The turbulence kinetic energy and its rate of dissipation are obtained from Appendix A2, equations 1, and 2.

3.1.4.2 Combustion model

Assuming equal diffusivities of fuel streams, which is acceptable for turbulent flow [46-48], the fluid thermochemistry can be simplified to conserved scalar quantity, the mixture fraction (f). The mixture fraction can be written in terms of the atomic mass fraction as Appendix A2, equation 3. The transport equation for is as Appendix A2, equation 4. ANSYS Fluent solves a conservation equation for the mixture fraction variance, $\overline{f'^2}$ is as Appendix A2, equation 5 where default values for the constants σ_t,C_g, and C_d are 0.85, 2.86, and 2.0, respectively [46-48]. In non-adiabatic system, the average scaler properties such as density-weighted mean species mass fractions, enthalpy, and temperature, can be calculated using probability density function as Appendix A2, equation 6 [46-48].

In practice, PF is unknown and is modeled as a mathematical beta function that approximates the actual PDF shapes based on experimentally observed PDFs [46-48].

3.1.5 Validation

The CFD BC model was validated against the published CFD simulation model by Bo Liu using the temperature profile along the burner axis form furnace bottom wall at elevation Z=0 m to Z=2 m as showed in Fig.27.

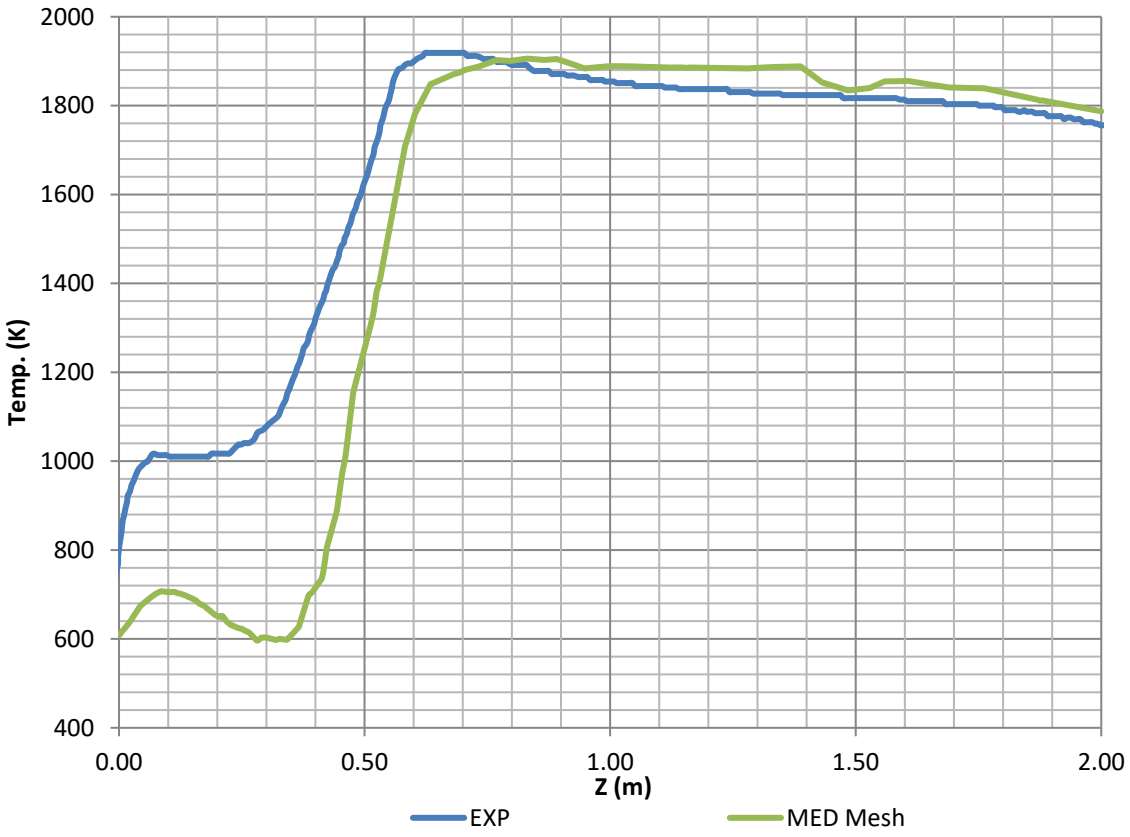

Figure 27.Temperature profile validation by MED mesh

The blue curve, Exp, represents Bo Liu's temperature profile. As illustrated in Fig. 27, the temperature profile increases slightly at 0<Z<0.1 m and stabilizes at 0<Z<0.2 as effect of the primary fuel combustion. The zone of 0<Z<0.2 is called inner recirculation zone (IRZ). Then there is significant increase in temperature at 0.2<Z<0.6 m due to the effect of the secondary fuel which represents around 75% of the total fuel supply. Then, form 0.6<Z<2 m temperature start to decease slightly as consumption of combusting reactants and radiation to furnace walls. Fig.28 shows the temperature contour of the furnace while Fig.29 shows a zooming in to the IRZ.

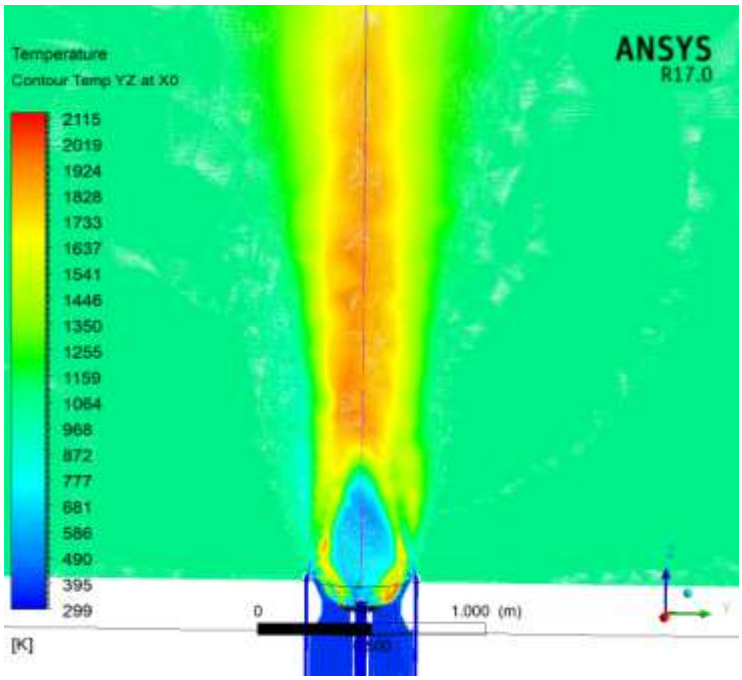

Figure 28.Furnace temperature contour

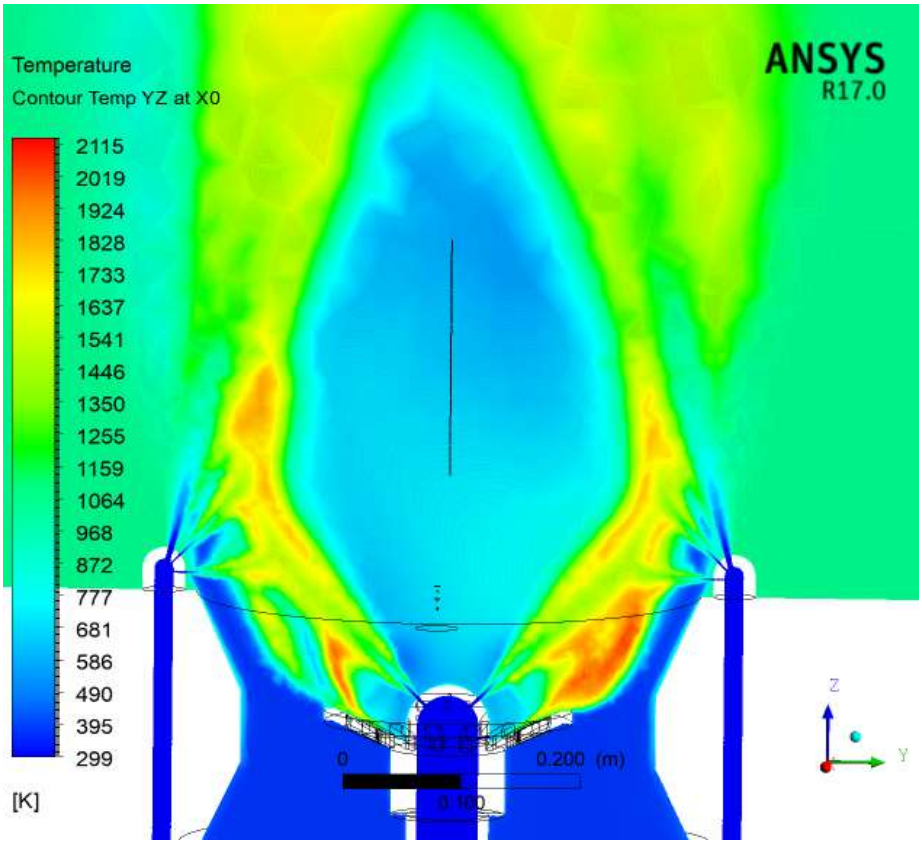

Figure 29.Burner IRZ

While MED Mesh curve represents our temperature profile. Both profiles are almost identical from Z=0.8m and higher. However, There is notable difference in temperature profile at elevations lower than Z=0.5m. The difference is due to the aforementioned differences in geometry regarding the elevation of primary fuel gun, secondary fuel guns and flame holder intersection with primary fuel diffusion.

The mesh confirmation test was done to confirm the independency of the solution on mesh size. Fig.30 shows two different meshes. The medium mesh (MED) with 5.2

million cells while the fine mesh (Fine) is 6 million cells.

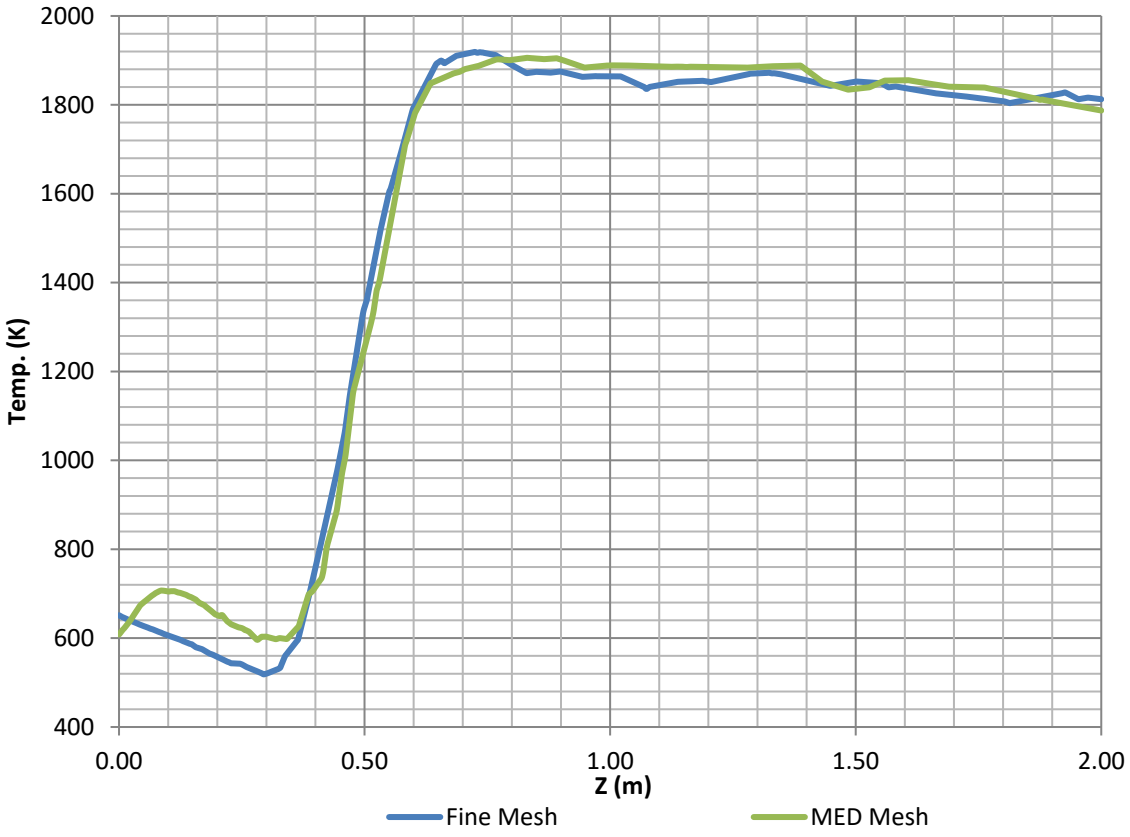

Figure 30.Temperature profile of MED and Fine mesh

Both meshes show a very close temperature profile with minor difference at 0<Z<0.3 around the IRZ. However, along the study, all simulations will be performed using the finer mesh with 6 million cells in order to capture as much details as possible at the IRZ. The model was done by two different radiation models, P1 and discrete ordinates (DO) models. Fig.31 shows comparison between those two radiation model and their effect on the temperature profile.

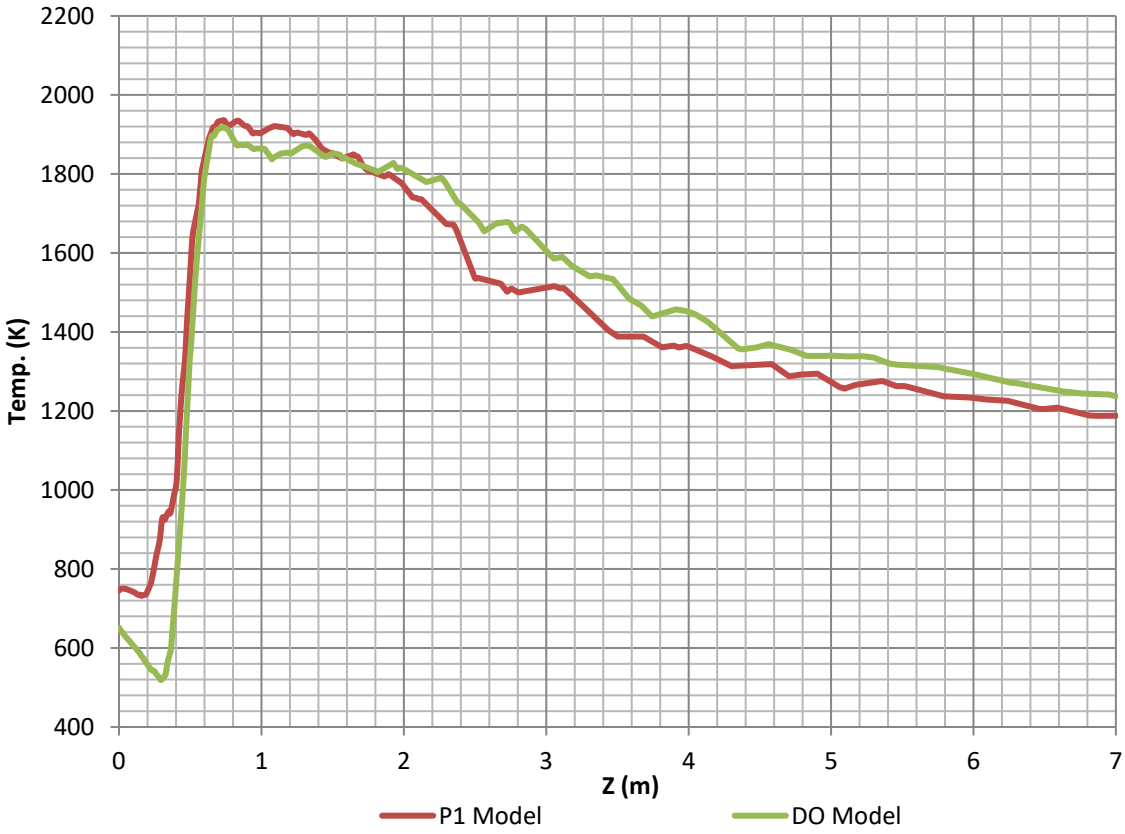

Figure 31.Temperature profile of P1 and DO model with Fine mesh

Both models showed a close temperature profile. However, DO model is more accurate in terms of predicting the radiative heat transfer by simplifiying the radiative transfer equation (RTE) to simultaneous partial deferential equations. On the other hand, P1 model reduces RTE to quite simpler partial deferential equation by expressing radiative intensity with generalized Fourier series and spherical harmonics [49]. Hence, DO model will be used along the study.

3.2 Preliminary Data: Ethylene Process Base Case

3.2.1 Ethylene Base Case

An Ethylene case study with a capacity of 900,000 tons / year of high grade ethylene was constructed based on front-end technology where the separation section is led by the de-ethanizer unit and its overhead product is fed to the acetylene hydrogenation unit [50]. Fig.32 represents the process flow diagram for the ethylene base case.

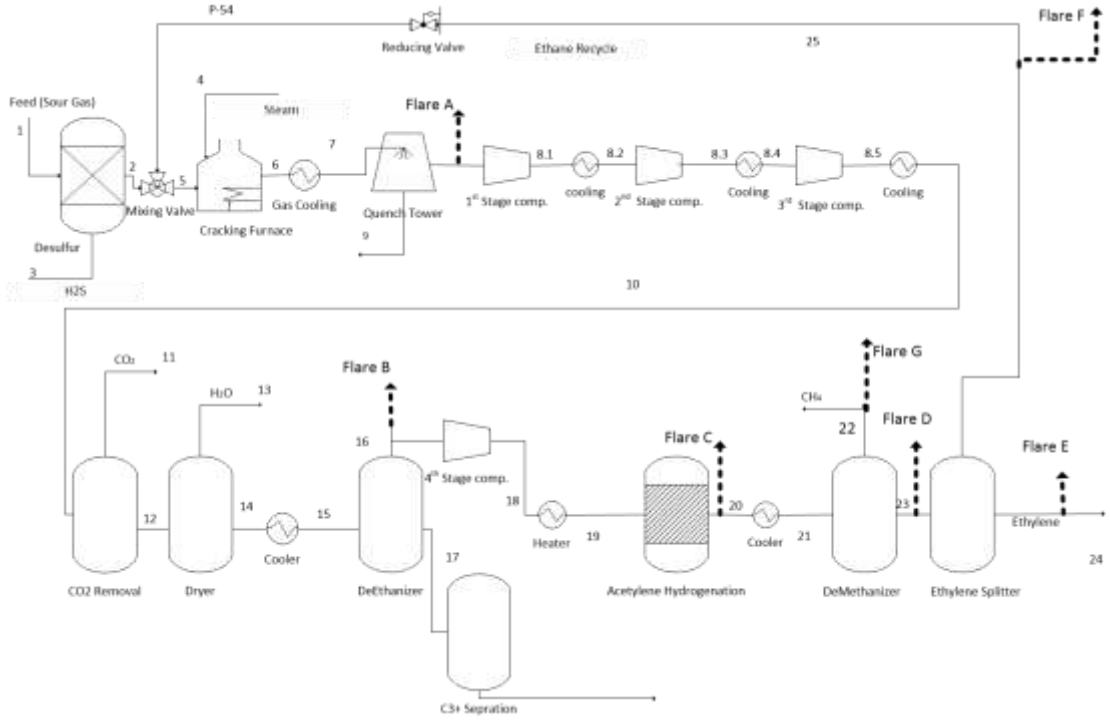

Figure 32.Process flow diagram, and major flaring sources in Ethylene process [50]

The raw feed stream contains 96 wt. % of ethane, 3 wt. % hydrogen sulfide, and 1 wt. % of carbon dioxide pass through desulfurization unit to remove hydrogen sulfide acid gas. Hydrogen sulfide concentration assumed to be reduced from 18pp, to 0 ppm. Sweet gas feed will be combined with recycled ethane stream and dilution steam before entering the cracking furnace in order to increase the furnace's yield and to avoid any carbon deposits (coke) forming. The gas to steam ratio in the feed is 3. Conversion and yield of the cracking furnace is 87.6% and 67.1% respectively. The selectivity is 76.6% based on yield and conversion. The outlet cracked gas stream will be cooled and enter quench tower for washing and further cooling. Quench tower outlet stream pass through multi

stage compression process and feed to caustic wash tower to remove carbon dioxide. The upstream from the caustic wash tower in vapor phase will be dehydrated in the dryers and feed to de-ethanizer column where C_2 and lighter components are being separated from the C_3 and heavier components. The net overhead from the de-ethanizer flows to an acetylene reactor where acetylene is being converted to ethylene. Acetylene reactor's conversion assumed to be 100%. The outlet stream enters de-methanizer column. De-methanizer's downstream to the C_2 Splitter to separate the mixed C_2 stream into an ethane recycled stream and the ethylene which is the main product.

3.2.2 Flaring in the Ethylene Process

Abnormal upsets associated with ethylene process include process startup and shutdown, insufficiencies in process compressors & refrigeration compressors, over pressurized vessels & columns, off-spec products and deviation from normal operating conditions [2, 51]. These process upsets and the flare locations that they impact for our base case ethylene plant were identified and validated by industrial experts. Fig.32 illustrates seven possible flare sources as bold dashed arrows in ethylene process base case [50]. Table 9 shows seven common abnormal scenarios in ethylene process and its associated flaring streams in ethylene process.

Table 9.Common Abnormal Scenarios in Ethylene Process [6]

Scenario	***Upset type***	***Attached flares***
1	All furnaces trip	A , B , C , D , E , F , G
2	CGC trip	A , B , C , D , E , F , G
3	PRC trip	A , B , C , D , E , F , G
4	Utility failure from supplier	A , B , C , D , E , F , G
5	Off-Spec	C , D , E
6	Acetylene reactor trip	C , D
7	Pump trip	D
8	Furnace shutdown	A

In the presented case, flaring scenario assumed to be 12 non-continuous hours per annum where flaring occurs from all flare sources A-G mentioned in Table 10. The detailed composition of each stream is presented in the appendix A3.

Table 10.Ethylene Case Study Flared Gas Streams Specifications [6]

Parameter	Unit	Flare Name						
		A	B	C	D	E	F	G
Mass Flow	ton/hr	190.6	171.1	171.1	124.6	102.7	21.9	46.5
Temperature	K	318.0	223.7	355.7	265.3	244.6	244.6	191.8
Pressure	psia	23.0	334.7	464.0	461.4	270.0	270.0	460.0

3.3 Tracking CO_2 Emissions

An in-house developed GHG calculator used in this study was based on European commission guidelines for the monitoring and reporting of greenhouse gas emissions [52]. This calculator can compute CO_2/CO_2-e emission both for the fuel combustion and flare steam combustion.

3.3.1 CO_2 Emissions Due to Fuel Combustion

The amount of emitted GHG gases like carbon dioxide, methane and nitrogen dioxide can be measured according to EU guidelines when fossil fuel is combusted. The following equation is used to calculate the GHG emissions:

$$CO_2 \text{ emissions} = \text{Activity data} \times [EF_{CO_2} + (EF_{CH_4} \times GWP_{CH_4}) + (EF_{N_2O} \times GWP_{N_2O})] \times \quad (1)$$

Oxidation factor

Activity Data = Fuel Consumed × NCV (2)

According to 2006 IPCC guidelines for national greenhouse gas inventories, the unit of activity data is TJ, fuel consumption is tons, NCV is TJ/ton and emission factor (EF) is tons CO_2/TJ while combustion oxidation factor represents the amount of oxidized carbon [53]. Oxidation factor should be set based on standardized method which is approved by competent authority [52]. In the absence of standardized values, a value of 1.00 can be assumed [53]. Global warming potential (GWP) values of CH4 and N_2O for 20 years are 56 and 280 respectively according to UN Climate Change website [54].

3.3.2 CO_2 Emissions Due to Flare Combustion

Industrial flaring can occur from single or multiple stream sources. Therefore, the CO_2/CO_2-e emissions at certain upset can be calculated from the summation of CO_2/CO_2-e emissions from the responsible flared gas stream sources. The following equations are used to estimate the CO_2/CO_2-e emissions for each upset:

$$\mathrm{CO_2} - \text{e emissions at Upset} = \sum \mathrm{CO_2} \text{ emissions from each flared gas stream} + \sum \mathrm{CH_4} \text{ emissions from each flared gas stream} \times \mathrm{GWP_{CH_4}} \quad (3)$$

$$\text{CO}_2 \text{ emissions from flared gas stream } = \dot{m} \times \text{duration}$$

$$\times\ \text{MW}_{\text{CO}_2}\left[\sum_{i}\frac{\text{X}_i}{\text{MW}_i}\times\ \text{Combustion Ratio}_i\times\ \text{CCF}_i\right] \quad (4)$$

$$\text{CH}_4 \text{ emissions from flared gas stream } = \dot{m} \times \text{duration} \times\ \text{X}_{\text{CH}_4}[1-\text{CCF}_i] \quad (5)$$

Conversion factor reflects the proportion of non-oxidized carbon and assumed equal for each flared gas stream. In absence of real data a value of 1.00 can be used [53].

3.4 Quantifying Energy Loss due to Flaring at Abnormal Situation (Upsets)

The energy content of any specific flare stream at variant mixture composition can be measured by Wobbe number, or Wobbe index (WI), which is a representative parameter for the effect of combustion energy output of variable fuel mixture and composition [55]. The following equations can be used to estimate the Wobbe index of certain hydrocarbon gas on a stream gas line[56]:

$$W_v\ (T_b) = \frac{H_v\ (T_b)}{\sqrt{d_v}} \tag{6}$$

$$H_v(T_b) = \frac{H_m\ (T_b) P_v}{R T_v\ Z_v} \tag{7}$$

$$H_m\ (T_b) = \sum_{i=1}^{N} y_i H_{mi}\ (T_b) \tag{8}$$

$$Z_v = 1 - \left(\sum_{i=1}^{N} y_i \sqrt{b_i} \right)^2 \tag{9}$$

$$d_v = \frac{z_{vL} M}{z_v M_L} \tag{10}$$

$$M = \sum_{i=1}^{N} y_i\ M_i \tag{11}$$

WI and relative density both can be estimated at combustion reference conditions using DIN standards [56]. The WI has units such as BTU per SCF or MJ per m3, however to avoid any possible confusion with the volumetric heating value of the gas, it is customary to represent WI as a unit-less quantity [57].

3.5 Evaluation of CO_2 Emissions Tax (Developed GHG Calculator)

The following formula can be used to evaluate CO_2 emissions tax:

$$\mathrm{CO_2e\ emissions\ tax\ (\$)} = \mathrm{CO_2e\ emissions\ (tons)} \times \mathrm{CO_2e\ price}\ \left(\frac{\$}{\mathrm{Ton\ CO_2e}}\right) \qquad (11)$$

Fig.33 illustrates the methodology for estimating CO_2 emissions, carbon tax and Wobbe Index (WI)

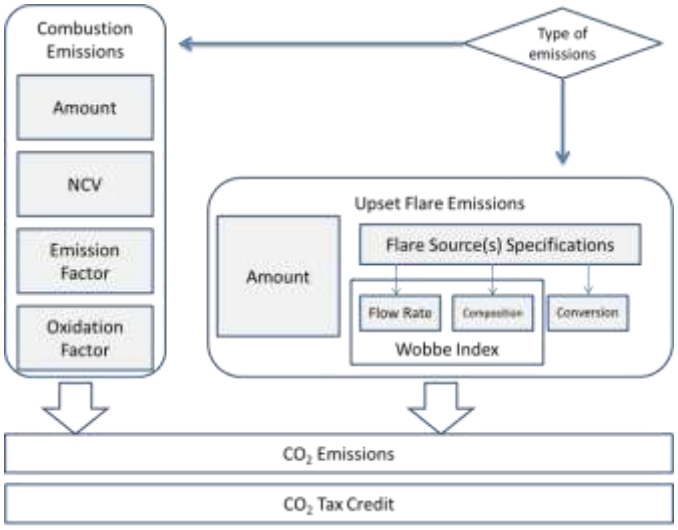

Figure 33.Methodology for estimating CO_2 emissions, carbon tax and Wobbe Index (WI)

CHAPTER 4: RESULTS & DISCUSSION

The CFD simulations main scope was to study the temperature profiles for various flare streams, composition, air and fuel mass flow, and excess air percentage. However, the boundary conditions of fuel and air temperatures, PF to SF mass flow ratio, furnace walls temperature and radiation were fixed along the study.

The composition, WI of each flare stream and flare mixture stream are stated in the appendices A3-A4. Each simulation case was performed till convergence with continuity residual below 10^{-2}, mass balance error below 0.15% and energy balance error below 3%. In average, the convergence happened around 4000-10000 iterations. Appendix A5 summarizes the air/fuel flow follow, WI, mass/energy balance differences and error percentages.

Then, each chart during the comparison between temperature profiles, the elevation along the burner axis was divided to four different zones. The first zone (0<Z<0.3-0.4 m) is the inner recalculation zone (IRZ) where the turbulence is at maximum due to air passage thru burner's flame holder and start of PF air mixture combustion. In Zone 2 (0.3-0.4<Z<0.6-0.8 m), the influence of SF combustion comes into effect and temperature peaks. Zone 3 (0.6-0.8<Z<1.3-2.5 m), starts from the peak temperature and continue with minor decline in temperatures. Then, the temperature declines gradually as combustion proceeds to its end where flue gas lose heat by radiation thru furnace walls in zone 4 (1.3-2.5<Z<7 m)

4.1 Effect of Fuel Inlets Flow at Constant Excess Air%

The BC model of methane fuel combustion was simulated with multiple flows of 2, 4, and 10 times BC fuel flow while excess air percentage and primary fuel to secondary fuel mass flow ratio are constants. Table 12 summarizes fuel and air flow boundary conditions.

Table 11.Fuel and Air Flow Boundary Conditions

SIMULATION	PF mass flow (g/s)	SF mass flow (g/s)	Total fuel mass flow (g/s)	Air mass flow (g/s)	Excess air (%)
BC FLOW	7.84	20	27.84	560	
2 TIMES BC FLOW	15.68	40	55.68	1120	
4 TIMES BC FLOW	31.36	80	111.36	2240	18.3%
10 TIMES BC FLOW	78.4	200	278.4	5600	

Fig.34 shows the temperature profile for the methane fuel combustion at aforementioned mass flow boundary conditions.

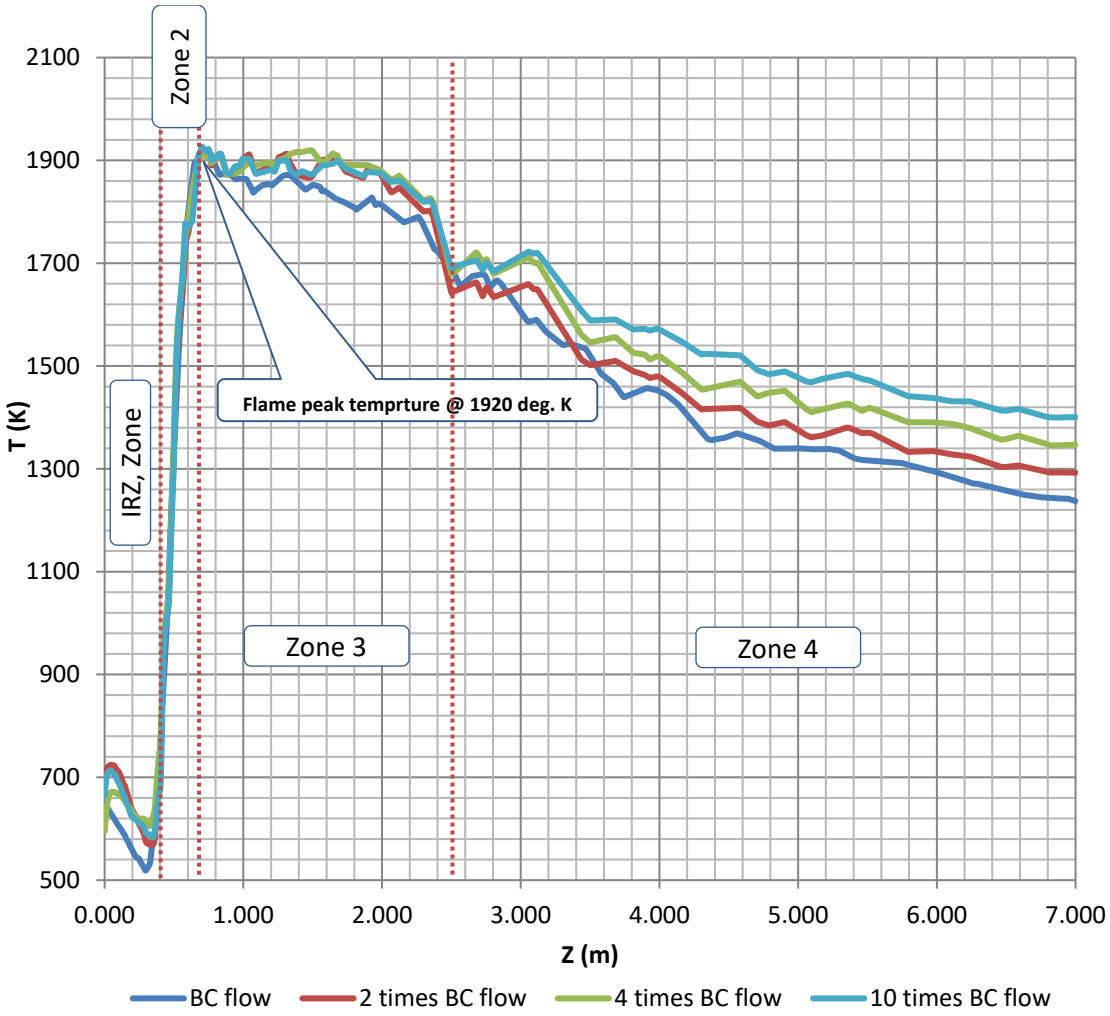

Figure 34.Temperature profile along burner axis for multiple inlets flow at constant excess air %

As shown in Fig.34, at all fuel flows, the temperature profiles deviate slightly at IRZ where 0<Z<0.4 m [zone 1]. At Z>0.4 m, zone 2 start point, the secondary fuel combustion come into effect and temperature of all fuel flows increased dramatically to flame peak temperature at 1920 degree K approximately where Z=0.7 m, zone 2 end point. The maximum flame temperature is an intensive property which depends on the composition of the fuel stream. Hence, the maximum flame temperature is the same at all fuel flows. At 0.7<Z<2.5, zone 3, the temperature profiles start to deviate from each other as combustion proceeds and reactants being consumed. At Z>2.5, zone 4, the deviation amplifies in a descending order. The lower the fuel flow the lower the temperature profile. This is explained as the higher flow the higher energy content and the higher excess of internal energy after losing portion to the furnace walls through radiation. The remaining internal energy is being reflected in the flue gas temperature.

4.2 Flare Streams as Fuel Source at Constant Fuel Mass Flow and Excess Air%

Each flare was used as a fuel source to the base case model. Fig.35 shows the temperature profile for the combustion of flare G and F with WI of 40.82 and 62.87.

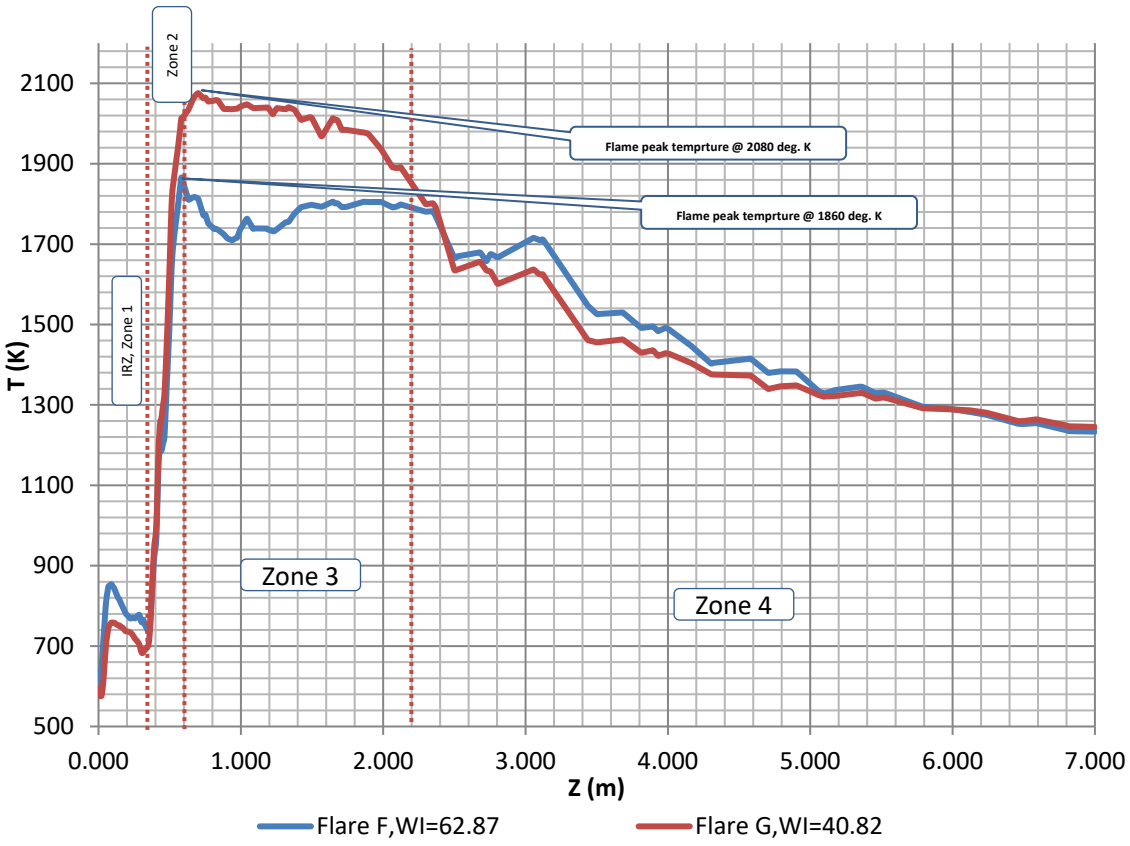

Figure 35.Temperature profile along burner axis for flares F & G at constant fuel flow and excess air %

Both flares showed different temperature profile especially at zone 3 where 0.6<Z<2.4 m. Flare F reached the peak temperature in relatively lower elevation (1680 deg. K at Z=0.6m) than flare G (2080 deg. K at Z=0.7m). At Z>2.2, flare G showed sharp decrease in temperature compared to flare F as a result of energy loss through heat radiation to the furnace walls.

Fig.36 shows the temperature profile for the combustion of flare A and B with WI of 47.14 and 49.37.

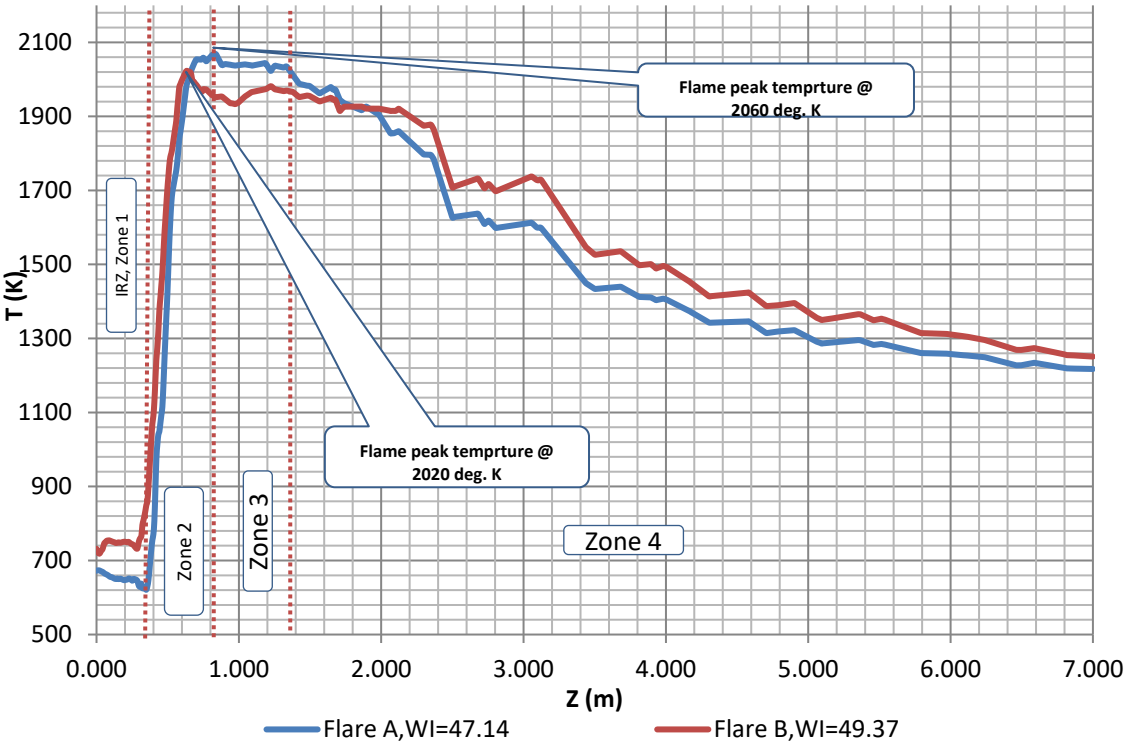

Figure 36.Temperature profile of fuel A and B

Again, both flares showed a relative difference in temperature profile. However flare A has lower WI, it showed higher peak temperature compared to flare B. On the other hand, at Z>1.4 m, temperature of both flares start to decrease as effect of radiation to furnace walls. Since flare A has lower WI, it showed a sharper temperature decline compared to flare B.

Fig.37 and 38 show the temperature profiles for two sets of flares with close WI. First set is Flare B & C with WIs of 49.37 and 49.47. Second set is flare E & D with WIs of 60.21 and 60.65 WI.

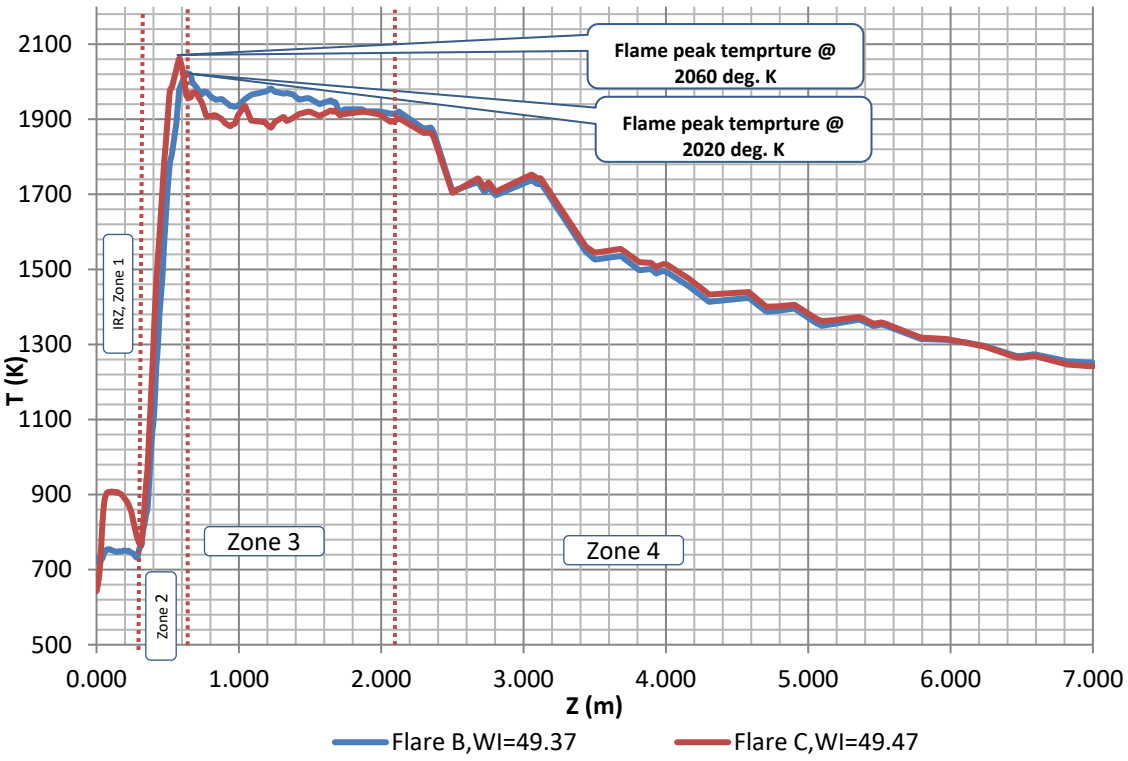

Figure 37.Temperature profile along burner axis for flares B & C at constant fuel flow and excess air %

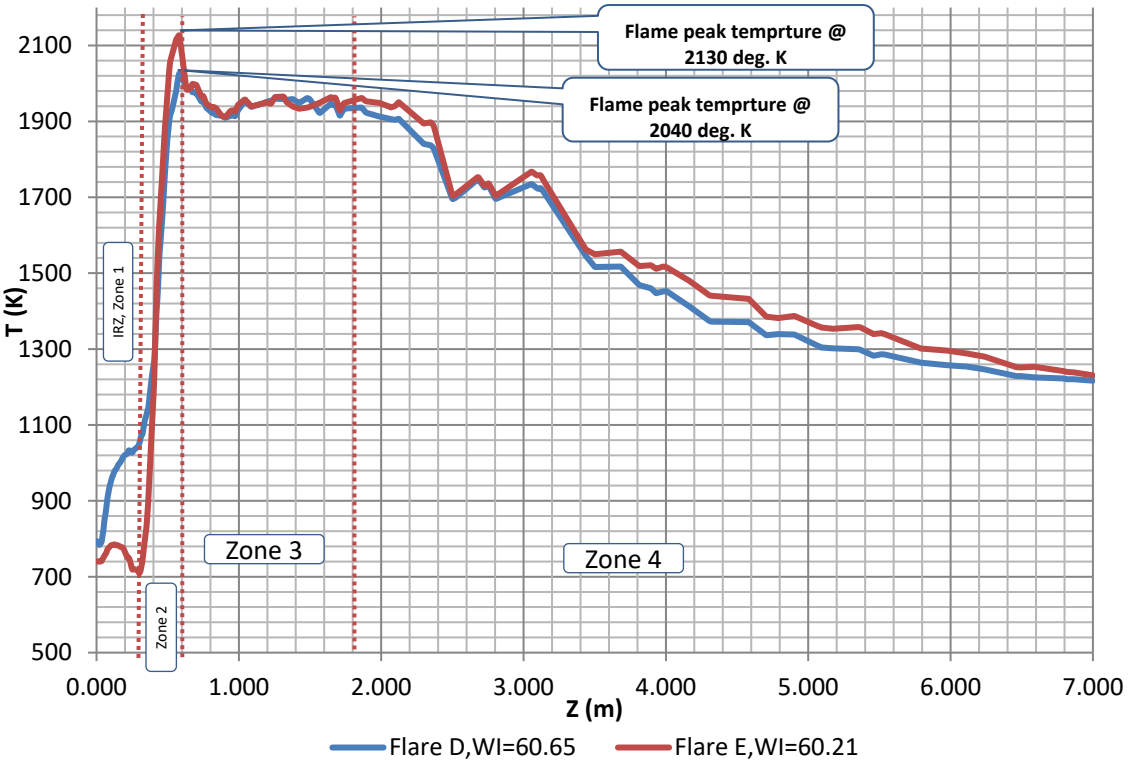

Figure 38.Temperature profile along burner axis for flares D & E at constant fuel flow and excess air %

In first set, flares B & C showed a very close temperature profile except at IRZ. In set two, both flares D & E showed relative difference in temperature profile compared to set one at Z>1.8 m. This is explained by comparing the flare streams composition of each set. In set one, flare B & C have a very close composition while in set two flare D & E have significant composition difference.

A comparison between two flares one from each set, flare B & E is showed in Fig.39.

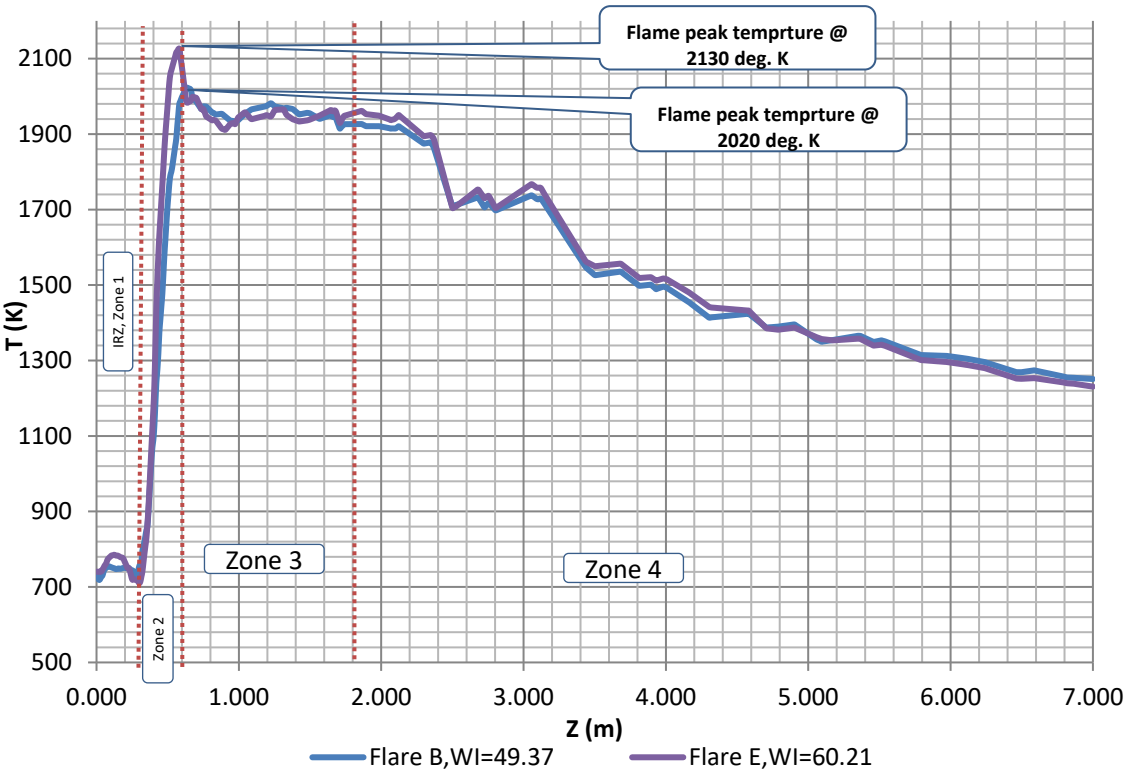

Figure 39.Temperature profile along burner axis for flares B & E at constant fuel flow and excess air %

Both flares have significant difference in WI as flare B WI is 49.37 while flare E WI is 60.21. Furthermore, their compositions are dissimilar. However, both flares showed a relatively close temperature profiles. A similar example presented in Fig.40 for flare A & G.

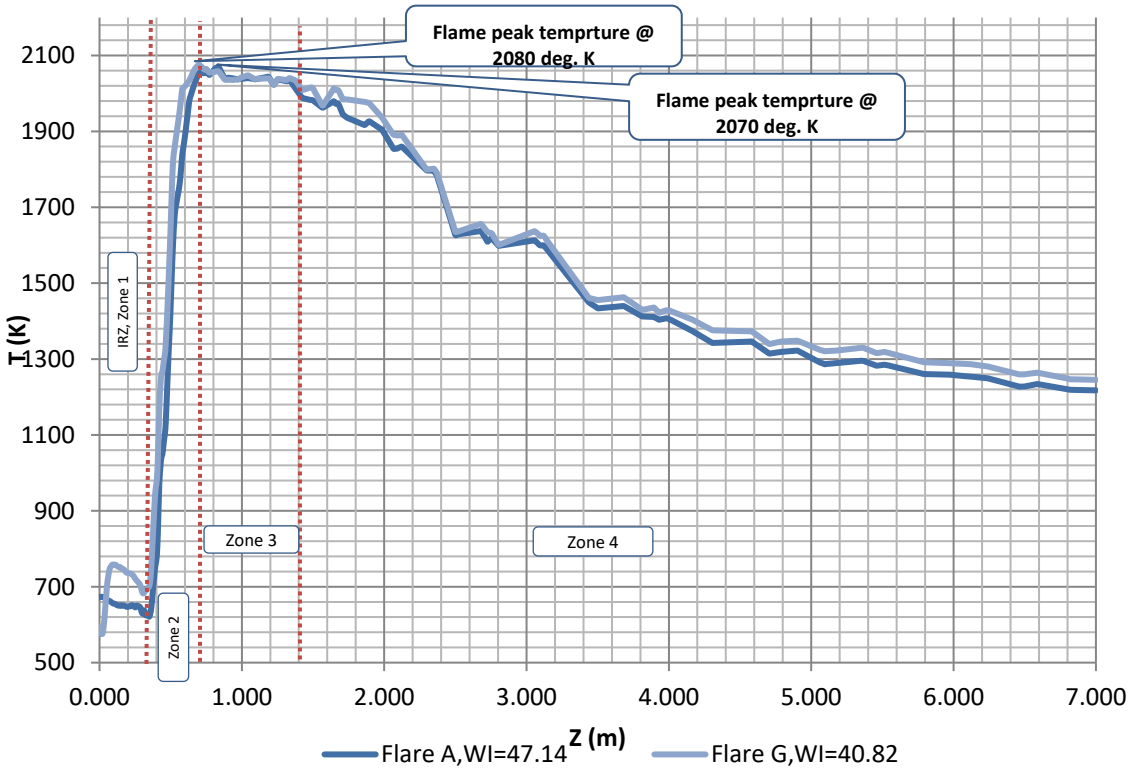

Figure 40.Temperature profile along burner axis for flares A & G at constant fuel flow and excess air %

Flare A & G have different have different composition and a variant WIs of 47.14 and 40.80 consequently. However, they showed a similar temperature profiles over the elevation of 0.7<Z<3.4 m.Hence, in the two previous examples, investigating how two streams different in composition and WI resulted in a close temperature profiles may answer how to utilize a mixture of two different flare streams in a cracking furnace while maintaining the necessary temperature profile for the cracking process.

4.3 Flare Mixture Streams as Fuel Source at Constant Fuel Mass Flow and Excess Air%

Flare mixtures of different composition were used as fuel source and simulated in our CFD model. The methodology of mixing flare streams was to find the optimum flare stream mixture WI to match NG WI which was the main fuel source in the ethylene base case. Fig.41 shows the temperature profile of each mixture.

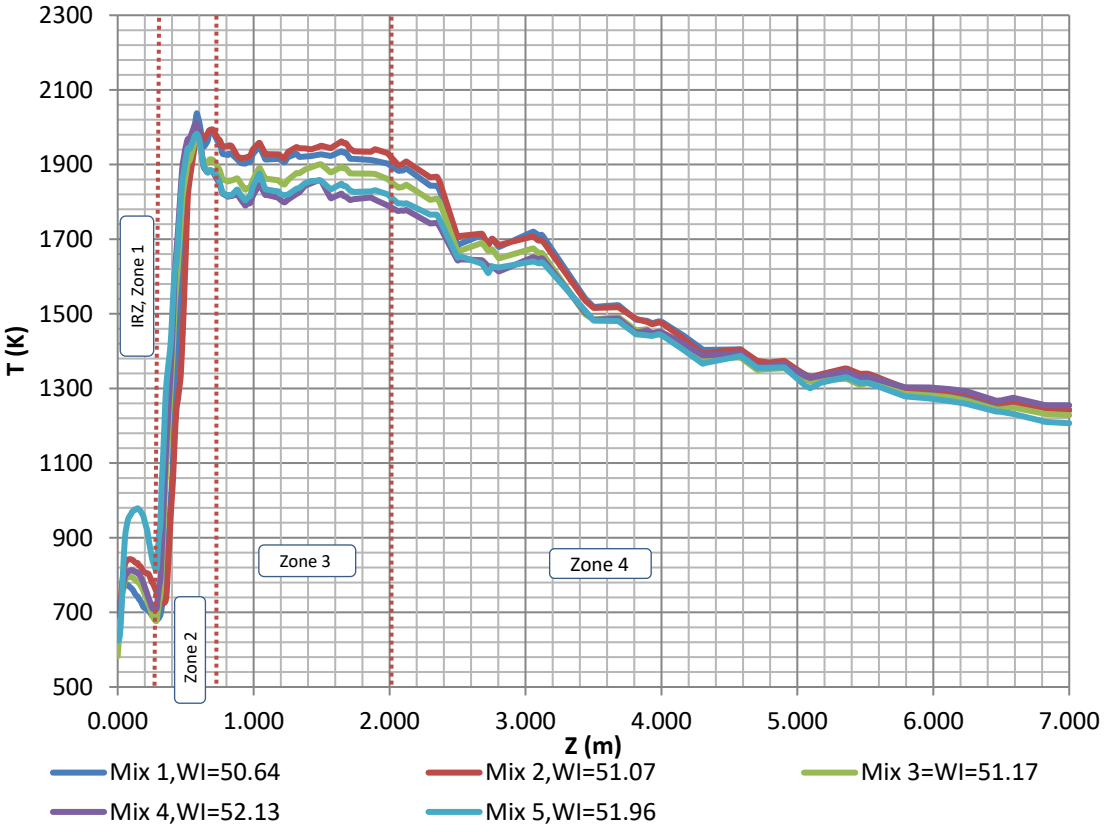

Figure 41.Temperature profile along burner axis for flare mixtures 1-5 at constant fuel mass flow and excess air %

Fig.42 shows the temperature profile for mixture 2 and 3 with WI of 51.07 and 51.17 consequently.

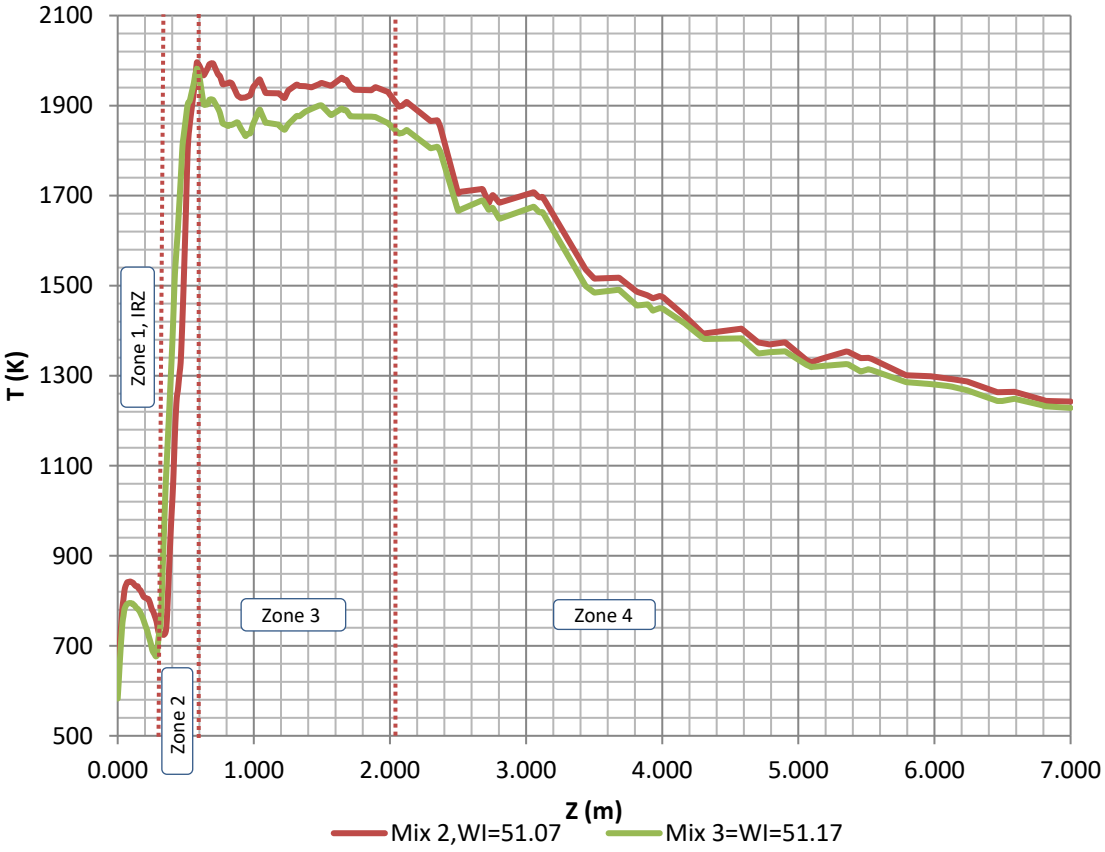

Figure 42.Temperature profile along burner axis for flares mixtures 2 & 3 at constant fuel flow and excess air %

Both mixtures showed slight difference in their temperature profile. However, their WI is significantly close. This is explained by the composition difference.

Fig.43 shows another temperature profiles for mixture 1 & 2.

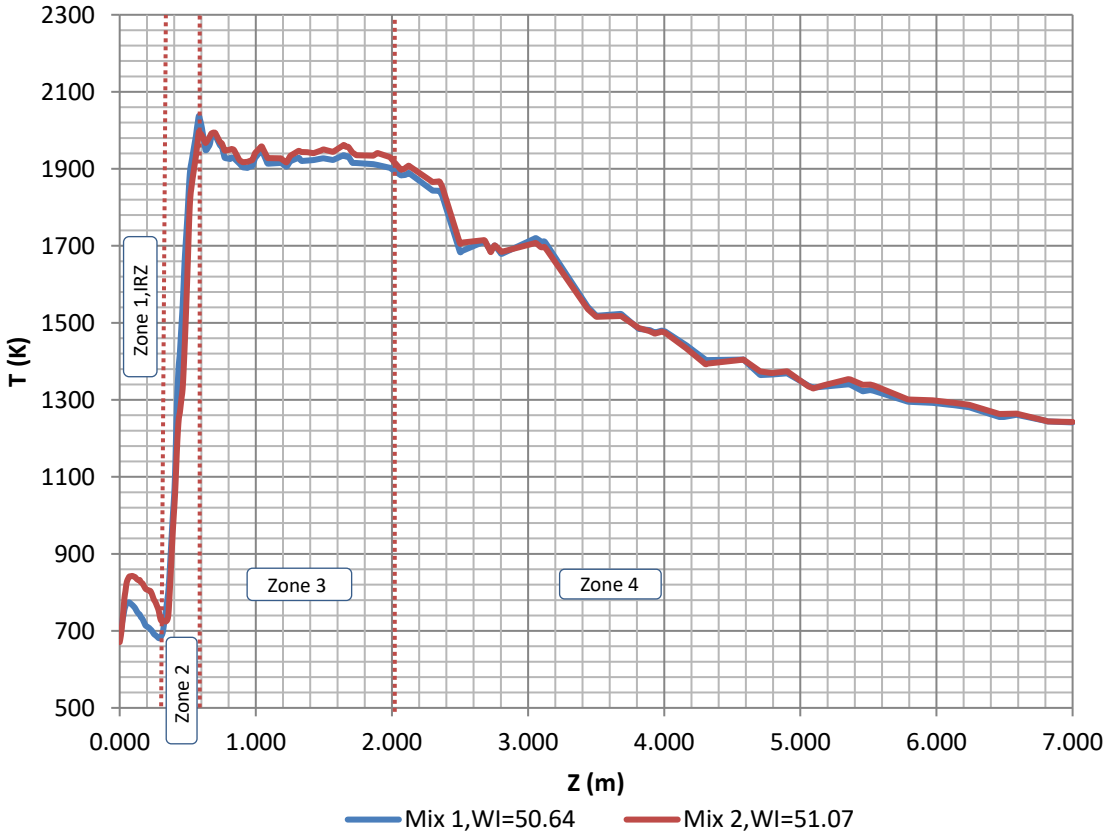

Figure 43.Temperature profile along burner axis for flares mixtures 1 & 2 at constant fuel flow and excess air %

Like flare sets (B, E) and (A,G), Mixture 1 and 2 have identical temperature profiles over many periods along the furnace elevation at Z>0.3m. However, they have considerable composition difference in terms of ethane and ethylene content.

4.4 Excess Air Effect on Temperature Profile Selected Flare Streams

In Fig.44, the BC fuel flow rate of 27.84 g/s was simulated with different excess air flow of 18.3%, 10% and stoichiometric air flow of 0%. It was expected that lowering the excess air will reduce the temperature dilution effect caused by flue gas heat loss to the excess air. Hence, temperature profile was expected to shift up and come close to the temperature profiles of the multiple fuel flow rates of 2, 4, or 10 times the fuel flow rate. However, at both excess air of 10 & 0%, the temperature profile declined sharply where the 10% excess air showed more negative slope than the 0% excess air.

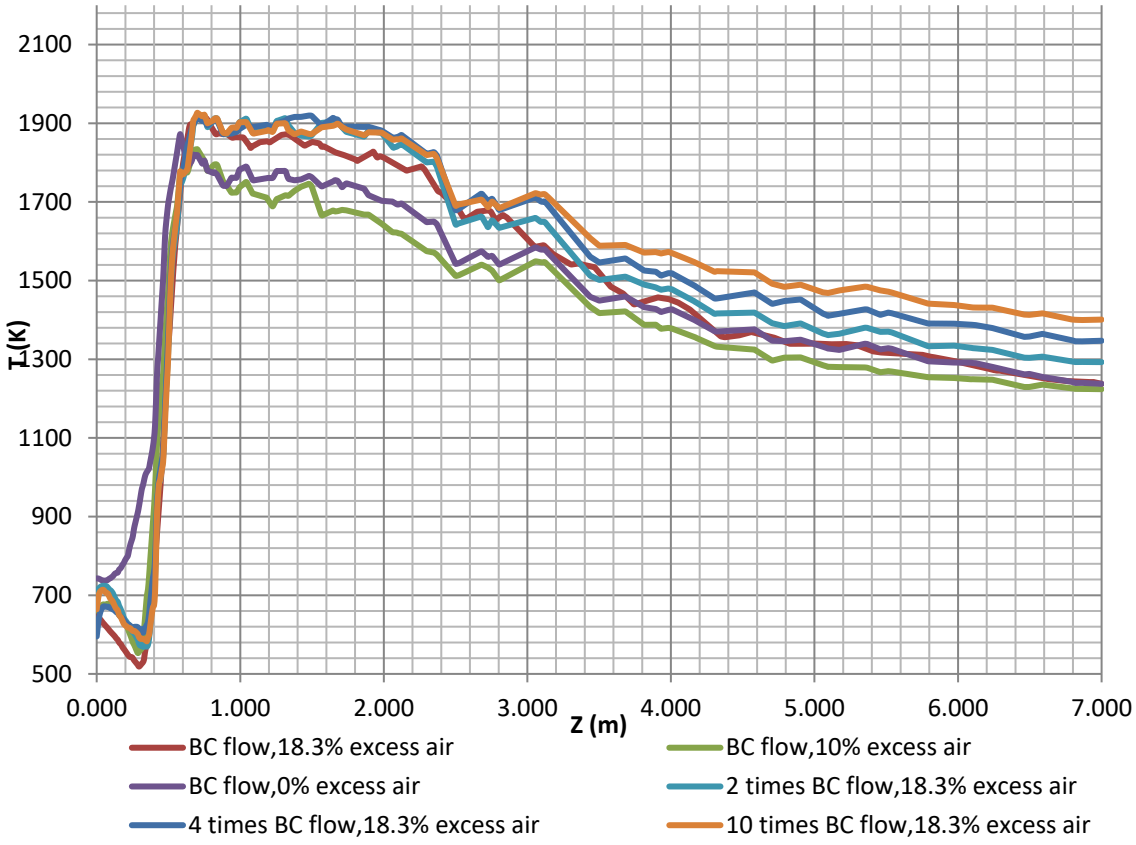

Figure 44.Temperature profiles along burner axis for BC at variant excess air % and multiple inlets flow

In Fig.45-46, Flare A and Mixture 4 were simulated with 18.3, 10 and 0 % excess air. Again, both excess air flows did not shift the temperature profile up as it was expected. In addition, in zone 2, the 10% excess air in Fig.45 showed closer temperature profile to the 18.3% excess air flow while in Fig.46 the 0% excess air showed a closer temperature profile to the 18.3% excess air.

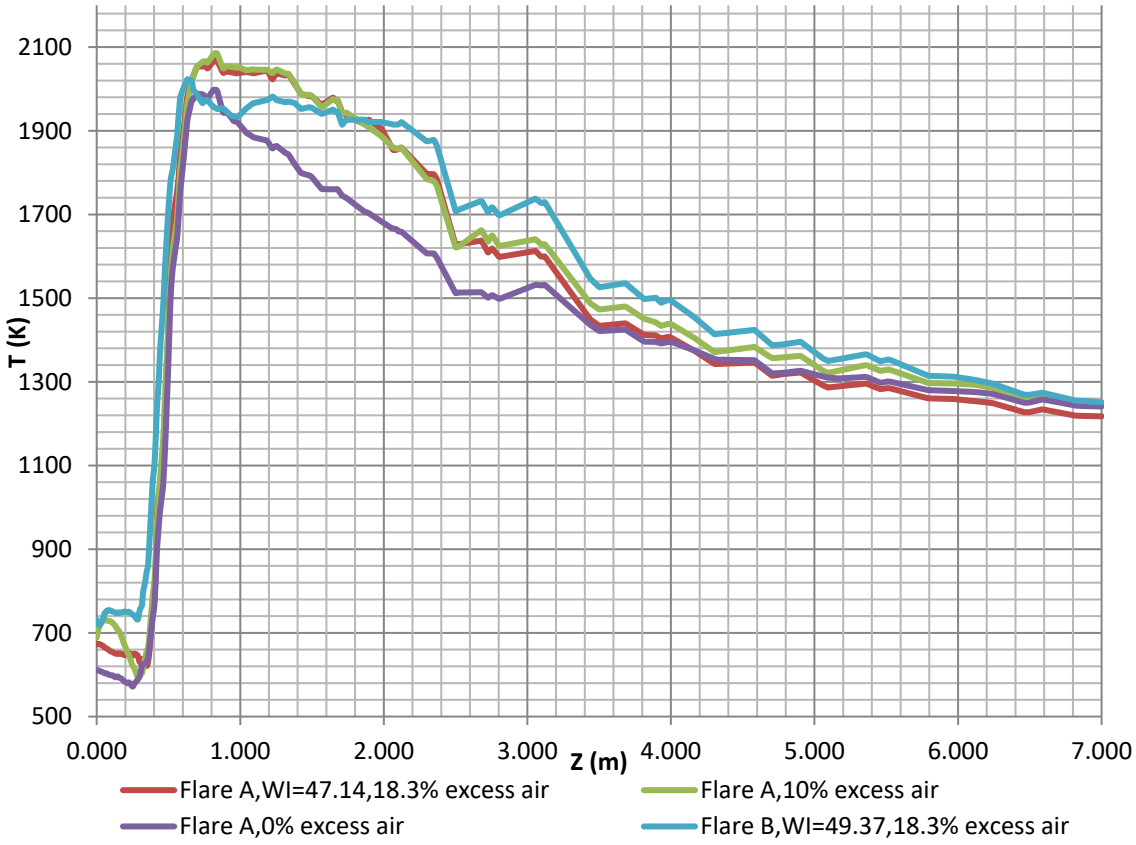

Figure 45.Temperature profile along burner axis for flare A at variant excess air % and flare B at 18.3% excess air

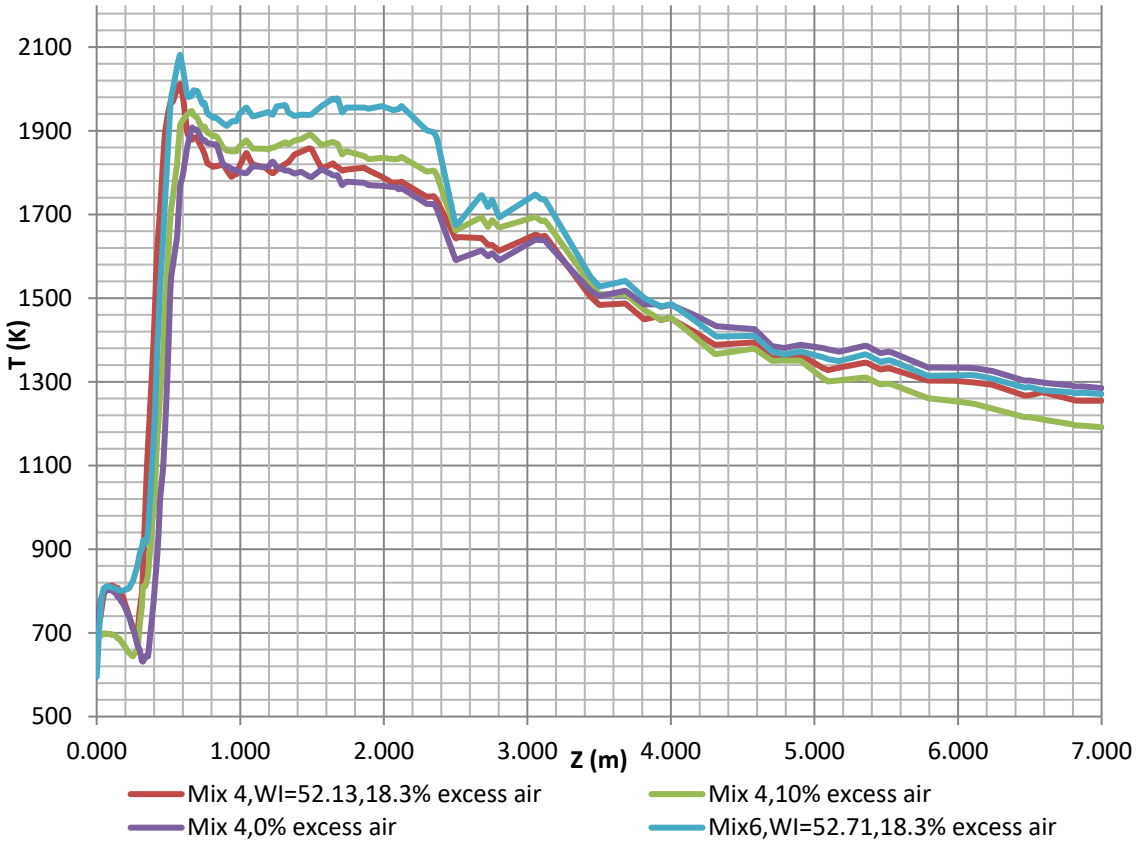

Figure 46.Temperature profile along burner axis for mixture 4 at variant excess air % and flare 6 at 18.3% excess air

Hence, the effect of excess air on temperature profile along the elevation is not mathematically predictable and it is required to be simulated and to be studied as case by case.

CHAPTER 5: CONCLUSION AND FUTURE WORK

This work has investigated the potential of recycling flared gas in an ethylene process to ethylene cracking furnace to manage flares from uncertain sources during abnormal situations. An ethylene base case study is studied to examine the applicability of the proposed methodology for flare utilization. A GHG calculator was developed to assess the carbon emission and WI of ethylene process potential flares. A CFD simulation was developed for a low NOx burner which is commonly used in industrial furnaces including the ethylene cracking furnaces. The developed simulation can assess the flue gas temperature, velocity, pressure, radiation and composition profiles. In addition, it can be used as a tool to test several burner geometries such as primary and secondary fuel number of guns, nozzle angle and height and tile shape. Furthermore, it can be integrated with any optimization framework for evaluating fuel supply alternatives. The main scope in this study was the temperature profile due to its significant influence on the cracking process which is the main function of the furnace.

The results demonstrated that utilizing a flared gas in an ethylene cracker can satisfy the temperature profile required for the cracking process. However, extra attention should be given to the mixing compositions, excess air ratios and heating values of the mixture. Having a fuel with similar heating value or WI will not result in similar temperature profile of existing fuel source. Using different excess air percentage has no linear effect on burner's temperature profile. Hence, in order to establish a frame work for mixing flare streams during abnormal situation, it is recommended to run multiple simulations of variant flare streams at variant excess air flows. Then, simulations with close temperature

profiles could be identified. In addition, based on process specific flaring profile, a median temperature profile could be developed as the main fuel gas source in basis of design of a new furnace as a preconstruction mitigation.

Further research could involve the impact of hydrogen composition, olefin and paraffinic content of fuel, and PF to SF mass flow ration on temperature profile. In addition, the effect of burner's geometry and staged fuel angle on the temperature profile of the racking furnace.

REFERENCES

1. Eljack, F.T., M.M. El-Halwagi, and Q. Xu, *An Integrated Approach to the Simultaneous Design and Operation of Industrial Facilities for Abnormal Situation Management.* Computer Aided Chemical Engineering, 2014. 34: p. 771-776.
2. Kazi, M.-K., et al., *Multi-objective optimization methodology to size cogeneration systems for managing flares from uncertain sources during abnormal process operations.* Computers & Chemical Engineering, 2015. 76(0): p. 76-86.
3. Eljack, F. and M.-K. Kazi, *Process safety and abnormal situation management.* Current Opinion in Chemical Engineering, 2016. 14: p. 35-41.
4. BANK, T.W. *New Gas Flaring Data Shows Mixed Results*. 2017 [cited 2017 12/7/2017]; Available from: http://www.worldbank.org/en/news/feature/2017/07/10/new-gas-flaring-data-shows-mixed-results.
5. Davoudi, M., et al., *The major sources of gas flaring and air contamination in the natural gas processing plants: A case study.* Journal of Natural Gas Science and Engineering, 2013. 13: p. 7-19.
6. Mohammed, F.M., et al., *Tracking of GHG Emissions and Tax Implication During Normal/Abnormal Situations – Ethylene Process Base Case Industrial Application*, in *Proceedings of the 4th International Gas Processing Symposium*. 2015, Elsevier: Oxford. p. 251-260.
7. Nations, U. *Kyoto Protocol*. 2014 [cited 2018; Available from:

http://unfccc.int/kyoto_protocol/items/2830.php.

8. Secretariat, I., *IPCC Factsheet: What is the IPCC?* 2013: Switzerland.
9. BANK, T.W. *Zero Routine Flaring by 2030*. 2017 [cited 2017 12/7/2017]; Available from: http://www.worldbank.org/en/programs/zero-routine-flaring-by-2030#1.
10. Change, U.N.F.C.o.C. *The Paris Agreement*. 2015 [cited 2018; Available from: http://unfccc.int/paris_agreement/items/9485.php.
11. Change, U.N.F.C.o.C. *Status of Ratification of the Kyoto Protocol*. 2015 [cited 2018; Available from: http://unfccc.int/kyoto_protocol/status_of_ratification/items/2613.php.
12. Bank, T.W. *Global Gas Flaring Reduction Partnership (GGFR).* [cited 2018; Available from: http://www.worldbank.org/en/programs/gasflaringreduction#4.
13. Change, U.N.F.C.o.C. *Paris Agreement - Status of Ratification*. [cited 2018; Available from: http://unfccc.int/paris_agreement/items/9444.php.
14. AlGhanim, N., M. Khraisheh, and F. Benyahia, *Flare Reduction Options and Simulation for the Qatari Oil and Gas Industry*, in *Proceedings of the 3rd Gas Processing Symposium*. 2012, Elsevier: Oxford. p. 7-14.
15. Raja, M., et al., *Qatargas Flare Reduction Program A2 - Al-Marri, Mohammed J*, in *Proceedings of the 4th International Gas Processing Symposium*, F.T. Eljack, Editor. 2015, Elsevier: Oxford. p. 261-271.
16. Abdulrahman, A.O., D. Huisingh, and W. Hafkamp, *Sustainability improvements in Egypt's oil & gas industry by implementation of flare gas recovery.* Journal of

Cleaner Production, 2015. 98: p. 116-122.

17. Gandler, T. *Steam Cracker Furnace Energy Improvements*. in *Industrial Energy Technology Conference*. 2010.

18. Charles E. Baukal, J., *Introduction*, in *Industrial Burners Handbook*, J. Charles E. Baukal, Editor. 2003, CRC Press.

19. Rahimpour, M.R. and S.M. Jokar, *Feasibility of flare gas reformation to practical energy in Farashband gas refinery: No gas flaring.* Journal of Hazardous Materials, 2012. 209–210(0): p. 204-217.

20. Emam, E.A., *GAS FLARING IN INDUSTRY: AN OVERVIEW.* Petroleum & Coal, 2015. 57(5): p. 532-555.

21. Kazi, M.-K., et al., *Integration of Energy and Wastewater Treatment Alternatives with Process Facilities To Manage Industrial Flares during Normal and Abnormal Operations: Multiobjective Extendible Optimization Framework.* Industrial & Engineering Chemistry Research, 2016. 55(7): p. 2020-2034.

22. Sadrameli, S.M., *Thermal/catalytic cracking of hydrocarbons for the production of olefins: A state-of-the-art review I: Thermal cracking review.* Fuel, 2015. 140: p. 102-115.

23. Engineering, C., *ETHYLENE PRODUCTION VIA CRACKING OF ETHANE-PROPANE*, in *Chemical Engineering*. 2015, Access Intelligence.

24. Charles E. Baukal, J., *Introduction*, in *The John Zink Hamworthy Combustion Handbook*, J. Charles E. Baukal, Editor. 2012, CRC Press

25. Inustruments, A.P., *Process Heaters, Furnaces and Fired Heaters*. Ametek

Process Inustruments.

26. Erwin Platvoet, D.B., and Rasik Patel, *Process Heaters*, in *The John Zink Hamworthy Combustion Handbook*, J. Charles E. Baukal, Editor. 2012, CRC Press

27. Jenkins, S., *Burner Inspection and Maintenance*, in *Chemical Engineering*. 2016, WWW.CHEMENGONLINE.COM: USA. p. 32.

28. Richard T. Waibel, M.G.C., and Bernd Reese, *Burner Design*, in *The John Zink Hamworthy Combustion Handbook*, J. Charles E. Baukal, Editor. 2012, CRC Press

29. Institute, A.P., *Burners for Fired Heaters in General Refinery Services*. 2014.

30. Jaime A. Erazo, J.a.T.M.K., *Burner Testing*, in *The John Zink Hamworthy Combustion Handbook*. 2012, CRC Press

31. Steve Londerville, J.C., and Charles E. Baukal, Jr., *Combustion Fundamentals*, in *The John Zink Hamworthy Combustion Handbook*, J. Charles E. Baukal, Editor. 2012, CRC Press

32. Joseph D. Smith, M.L., Eric M. Hixson, and Tom Eldredge, *CFD in Burner Development*, in *Industrial Burners Handbook*, J. Charles E. Baukal, Editor. 2003, CRC Press.

33. Peter F. Barry, S.L.S., and Steve Londerville, *Duct Burners*, in *The John Zink Hamworthy Combustion Handbook*, J. Charles E. Baukal, Editor. 2012, CRC Press

34. AlNouss, A., et al., *Integrated Data (i-Data), Mining and Utilization Approach*

for Effective Flare Management Strategies. Industrial & Engineering Chemistry Research, 2017. 56(10): p. 2789-2803.

35. *CTC*. 2014 July 28,2014 [cited 2014 July 31,2014]; Available from: http://www.carbontax.org/services/where-carbon-is-taxed/.

36. *B. C. Ministry of Finance*, B.a.f.p.-. 2015/16, Editor. 2013, National Library of Canada Cataloguing in Publication Data. p. 130.

37. Jiang, Z. and S. Shao, *Distributional effects of a carbon tax on Chinese households: A case of Shanghai.* Energy Policy, 2014(0).

38. He, Y., L. Wang, and J. Wang, *Cap-and-trade vs. carbon taxes: A quantitative comparison from a generation expansion planning perspective.* Computers & Industrial Engineering, 2012. 63(3): p. 708-716.

39. *Post-2020 reform of the EU Emissions Trading System*. 2015, Post-2020 reform of the EU Emissions Trading System. p. 9.

40. Klepper, G., *The future of the European Emission Trading System and the Clean Development Mechanism in a post-Kyoto world.* Energy Economics, 2011. 33(4): p. 687-698.

41. *Carbon Emissions Historical Data*. 2016 [cited 2016 May 13, 2016]; Available from: http://www.investing.com/commodities/carbon-emissions-historical-data.

42. Keohane, N.O., *Cap and Trade, Rehabilitated: Using Tradable Permits to Control U.S. Greenhouse Gases.* Review of Environmental Economics and Policy, 2009. 3(1): p. 42-62.

43. *Australia votes to repeal carbon tax*. 2014 July 17, 2014 [cited 2014 July

31,2014]; Available from: http://www.bbc.com/news/world-asia-28339663.

44. SIEGEL, M. *Australian parliament repeals carbon tax, emissions trading scheme*. 2014 [cited 2014 July 31, 2014]; Available from: http://www.reuters.com/article/2014/07/18/us-australia-carbon-vote-idUSKBN0FM04J20140718.

45. Anomohanran, O., *Determination of greenhouse gas emission resulting from gas flaring activities in Nigeria.* Energy Policy, 2012. 45(0): p. 666-670.

46. Liu, B., et al., *Numerical simulation of flow, combustion and NO emission of a fuel-staged industrial gas burner.* Journal of the Energy Institute, 2012.

47. Bo, L., X. Hong, and W. Yuan-Hua, *Numerical Study of the Effect of Staged Gun and Quarl on the Performance of Low-NOx Burners.* 2016.

48. ANSYS, I., *ANSYS Help Viewer*. 2017.

49. Chen, M.A.L.a.S.X., *CFD-Based Combustion Modeling*, in *The John Zink Hamworthy Combustion Handbook*, J. Charles E. Baukal, Editor. 2012, CRC Press

50. Kamrava, S., et al., *Managing abnormal operation through process integration and cogeneration systems.* Clean Technologies and Environmental Policy, 2014: p. 1-10.

51. Jokar, S.M., M.R. Rahimpour, and A. Shariati, *Heat exchanger application for environmental problem-reducing in flare systems of an oil refinery and a petrochemical plant: Two case studies.* Applied Thermal Engineering, 2016. 106: p. 796-810.

52. *Directive 2007/589/EC*. Official Journal of the European Union, 2007. 50, 85.

53. eggleston, s., et al., *Energy*, in *2006 IPCC Guidelines for National Greenhouse Gas Inventories*. 2006, Intergovernmental Panel on Climate Change (IPCC): Japan.

54. *United Nations Framework Convention on Climate Change*. 2014 [cited 2015; Available from: http://unfccc.int/ghg_data/items/3825.php.

55. Ranga Dinesh, K.K.J., X. Jiang, and J.A. van Oijen, *Hydrogen-enriched non-premixed jet flames: Analysis of the flame surface, flame normal, flame index and Wobbe index.* International Journal of Hydrogen Energy, 2014. 39(12): p. 6753-6763.

56. Standardization, D.G.I.f., *Calculation of superior and inferior calorific value, density and Wobbe index of gaseous fuels and other gases*. 1997, DIN German Institute for Standardization: Berlin.

57. *The Wobbe Index and Natural Gas Interchangeability*. 2007, Emerson Process Management. p. 2.

APPENDICES

Appendix A1.Cartesian Set of Differential Equations Solved in CFD [32]

$$-\frac{\partial(\overline{\rho}\tilde{u}\phi)}{\partial x}+\frac{\partial(\overline{\rho}\tilde{v}\phi)}{\partial y}+\frac{\partial(\overline{\rho}\tilde{w}\phi)}{\partial z}-\frac{\partial}{\partial x}\left(\Gamma_\phi\frac{\partial(\phi)}{\partial x}\right)-\frac{\partial}{\partial y}\left(\Gamma_\phi\frac{\partial(\phi)}{\partial y}\right)-\frac{\partial}{\partial z}\left(\Gamma_\phi\frac{\partial(\phi)}{\partial z}\right)=S_\phi$$

Equation	ϕ	Γ_ϕ	S_ϕ
Continuity	1	0	0
X-momentum	$\tilde{u}$	μ_e	$-\frac{\partial p}{\partial x}+\frac{\partial}{\partial x}\left(\mu_e\frac{\partial\tilde{u}}{\partial x}\right)+\frac{\partial}{\partial y}\left(\mu_e\frac{\partial\tilde{v}}{\partial x}\right)+\frac{\partial}{\partial z}\left(\mu_e\frac{\partial\tilde{w}}{\partial x}\right)+\overline{\rho}g_x-\frac{2}{3}\overline{\rho}\tilde{k}$
Y-momentum	$\tilde{v}$	μ_e	$-\frac{\partial p}{\partial y}+\frac{\partial}{\partial x}\left(\mu_e\frac{\partial\tilde{u}}{\partial y}\right)+\frac{\partial}{\partial y}\left(\mu_e\frac{\partial\tilde{v}}{\partial y}\right)+\frac{\partial}{\partial z}\left(\mu_e\frac{\partial\tilde{w}}{\partial y}\right)+\overline{\rho}g_y-\frac{2}{3}\overline{\rho}\tilde{k}$
Z-momentum	$\tilde{w}$	μ_e	$-\frac{\partial p}{\partial z}+\frac{\partial}{\partial x}\left(\mu_e\frac{\partial\tilde{u}}{\partial z}\right)+\frac{\partial}{\partial y}\left(\mu_e\frac{\partial\tilde{v}}{\partial z}\right)+\frac{\partial}{\partial z}\left(\mu_e\frac{\partial\tilde{w}}{\partial z}\right)+\overline{\rho}g_z-\frac{2}{3}\overline{\rho}\tilde{k}$
Mixture fraction	$\tilde{f}$	$\frac{\mu_e}{\sigma_f}$	0
Mixture fraction variance	$\tilde{g}$	$\frac{\mu_e}{\sigma_g}$	$-\frac{C_{g1}\mu_e}{\sigma_g}+\left[\left(\frac{\partial\tilde{f}}{\partial x}\right)^2+\left(\frac{\partial\tilde{f}}{\partial y}\right)^2+\left(\frac{\partial\tilde{f}}{\partial z}\right)^2\right]-C_{g2}\overline{\rho}\tilde{g}\frac{\tilde{\varepsilon}}{\tilde{k}}$
Turbulent energy	$\tilde{k}$	$\frac{\mu_e}{\sigma_k}$	$G-\overline{\rho}\tilde{\varepsilon}$
Dissipation rate	$\tilde{\varepsilon}$	$\frac{\mu_e}{\sigma_\varepsilon}$	$\left(\frac{\tilde{\varepsilon}}{\tilde{k}}\right)(c_1G-c_2\overline{\rho}\tilde{\varepsilon})$

where:

$$G=\mu_e\left\{2\left[\left(\frac{\partial\tilde{u}}{\partial x}\right)^2+\left(\frac{\partial\tilde{v}}{\partial y}\right)^2+\left(\frac{\partial\tilde{w}}{\partial z}\right)^2\right]+\left(\frac{\partial\tilde{u}}{\partial y}+\frac{\partial\tilde{v}}{\partial x}\right)^2+\left(\frac{\partial\tilde{u}}{\partial x}+\frac{\partial\tilde{w}}{\partial x}\right)^2+\left(\frac{\partial\tilde{v}}{\partial x}+\frac{\partial\tilde{w}}{\partial y}\right)^2\right\}$$

Appendix A2.Main Equations for Solving CFD Model

$$\frac{\partial}{\partial t}(\rho k)+\frac{\partial}{\partial x_i}(\rho k u_i)=\frac{\partial}{\partial x_j}\left[\left(\mu+\frac{\mu_t}{\sigma_k}\right)\frac{\partial k}{\partial x_j}\right]+G_k+G_b-\rho\varepsilon-Y_M+S_k \quad (1)$$

$$\frac{\partial}{\partial t}(\rho\varepsilon)+\frac{\partial}{\partial x_i}(\rho\varepsilon u_i)=\frac{\partial}{\partial x_j}\left[\left(\mu+\frac{\mu_t}{\sigma_\varepsilon}\right)\frac{\partial \varepsilon}{\partial x_j}\right]+C_{1\varepsilon}\frac{\varepsilon}{k}(G_k+C_{3\varepsilon}G_b)-C_{2\varepsilon}\rho\frac{\varepsilon^2}{k}+S_\varepsilon \quad (2)$$

$$f=\frac{Z_i-Z_{i,ox}}{Z_{i,fuel}-Z_{i,ox}} \quad (3)$$

$$\frac{\partial}{\partial t}(\rho\bar{f})+\nabla\cdot(\rho\vec{v}\bar{f})=\nabla\cdot\left(\left(\frac{k}{C_p}+\frac{\mu_t}{\sigma_t}\right)\nabla\bar{f}\right)+S_m+S_{user} \quad (4)$$

$$\frac{\partial}{\partial t}(\rho\overline{f'^2})+\nabla\cdot(\rho\vec{v}\overline{f'^2})=\nabla\cdot\left(\left(\frac{k}{C_p}+\frac{\mu_t}{\sigma_t}\right)\nabla\overline{f'^2}\right)+C_g\mu_t\cdot(\nabla\bar{f})^2-C_d\rho\frac{\varepsilon}{k}\overline{f'^2}+S_{user} \quad (5)$$

$$\bar{\phi}_i=\int_0^1 p(f)\phi_i(f)df \quad (6)$$

Where

Z_i: elemental mass fraction

Subscript ox: oxidizer stream inlet

Subscript $fuel$: fuel stream inlet.

K: Laminar thermal conductivity of the mixture

C_p: Mixture specific heat

σ_t: Prandtl number

μ_t: Turbulent viscosity.

Appendix A3.Flare A-G Stream Temperature, Pressure, Flow Rate, WI and Composition

Fuel			Flare A	Flare B	Flare C	Flare D	Flare E	Flare F	Flare G	Flare NG
T (K)			318	224	356	265	245	245	192	
P (Psia)			23	335	464	461	270	270	460	
WI			47.14	49.37	49.47	60.65	60.21	62.87	40.82	47.06
Mass flow ate (Kg/h)			190591	171115	171115	124613	102740	21873	46503	1108
Composition	Hydrogen	H2	0.0484	0.0539	0.0530	0.0000	0.0000	0.0000	0.1952	0.0000
	Methane	CH4	0.0821	0.0914	0.0914	0.0000	0.0000	0.0000	0.3365	0.8345
	Acetylene	C2H2	0.0105	0.0117	0.0000	0.0000	0.0000	0.0000	0.0000	0.0000
	Ethylene	C2H4	0.6401	0.7129	0.7255	0.8245	1.0000	0.0000	0.4604	0.0000
	Ethane	C2H6	0.1175	0.1300	0.1300	0.1755	0.0000	1.0000	0.0079	0.0729
	Propadiene	C3H4	0.0010	0.0000	0.0000	0.0000	0.0000	0.0000	0.0000	0.0000
	Propene	C3H6	0.0105	0.0000	0.0000	0.0000	0.0000	0.0000	0.0000	0.0000
	Propane	C3H8	0.0000	0.0000	0.0000	0.0000	0.0000	0.0000	0.0000	0.0201
	12-Butadiene	C4H6	0.0143	0.0000	0.0000	0.0000	0.0000	0.0000	0.0000	0.0000
	Butane	C4H10	0.0000	0.0000	0.0000	0.0000	0.0000	0.0000	0.0000	0.0103
	VinylAcetate	C4H6O2	0.0029	0.0000	0.0000	0.0000	0.0000	0.0000	0.0000	0.0000
	Cyclopentene	C5H8	0.0048	0.0000	0.0000	0.0000	0.0000	0.0000	0.0000	0.0000
	Pentane	C5H12	0.0000	0.0000	0.0000	0.0000	0.0000	0.0000	0.0000	0.0016
	Benzene	C6H6	0.0114	0.0000	0.0000	0.0000	0.0000	0.0000	0.0000	0.0000
	Hexane	C6H12	0.0000	0.0000	0.0000	0.0000	0.0000	0.0000	0.0000	0.0015
	Carbon Dioxide	CO2	0.0001	0.0000	0.0000	0.0000	0.0000	0.0000	0.0000	0.0126
	Water	H2O	0.0565	0.0000	0.0000	0.0000	0.0000	0.0000	0.0000	0.0000
	Nitrogen	N2	0.0000	0.0000	0.0000	0.0000	0.0000	0.0000	0.0000	0.0456
	Oxygen	O2	0.0000	0.0000	0.0000	0.0000	0.0000	0.0000	0.0000	0.0009
	Sum.		1.0000	1.0000	1.0000	1.0000	1.0000	1.0000	1.0000	1.0000

Appendix A4.Fuel Mixture Composition

Component	Mix 1	Mix 2	Mix 3	Mix 4	Mix 5
WI	50.64	51.07	51.17	52.13	51.96
Component			Xi		
C2H6	0.16	0.16	0.14	0.17	0.18
C2H4	0.48	0.52	0.41	0.52	0.53
CH4	0.31	0.26	0.38	0.26	0.23
H2	0.03	0.05	0.03	0.03	0.04
C3H8	0.01	0	0.01		0
H2O	0	0	0	0.01	0.01
N2	0.01	0.01	0.03	0.01	0.01
Sum	1	1	1	1	1

Appendix A5.Fuel / Air Flow and Mass / Energy Balance Errors for Each Simulation Case

Simulation \ Data	PF	SF	Air	Total	Mass balance error	Mass balance error	Combustion energy	Energy balance error	Energy balance error
	g/s					%	Kw		%
BC flow,18.3% exs air	7.84	20.0	560.0	587.84	0.05	0.01	1408.8	13.70	0.97
BC flow,10% exs air	7.84	20.0	520.9	548.74	0.21	0.04	1392.7	6.10	0.44
BC flow,0% exs air	7.84	20.0	473.5	501.34	0.22	0.04	1374.9	30.60	2.23
2X flow,18.3% exs air	16.68	40.0	1120.0	1176.68	0.14	0.01	2744.0	55.70	2.03
4X flow,18.3% exs air	31.36	80.0	2240.0	2351.36	2.60	0.11	5577.3	26.10	0.47
10X flow,18.3% exs air	78.40	200.0	5600.0	5878.40	1.50	0.03	13922.9	59.60	0.43
Flare A,WI=47.14	7.84	20.0	494.0	521.84	0.05	0.01	1341.1	1.00	0.07
Flare A,10% exs air	7.84	20.0	459.4	487.24	0.31	0.06	1340.6	22	1.6
Flare A,0% exs air	7.84	20.0	417.6	445.44	0.7	0.16	1333.1	12	0.9
Flare B,WI=49.37	7.84	20.0	527.0	554.84	0.36	0.06	1316.7	16.30	1.24
Flare C,WI=49.47	7.84	20.0	526.9	554.74	0.49	0.09	1327.1	7.60	0.57
Flare D,WI=60.65	7.84	20.0	488.2	516.04	0.21	0.04	1316.0	1.40	0.11
Flare E,WI=60.21	7.84	20.0	480.6	508.44	0.06	0.01	1313.0	7.20	0.55
Flare F,WI=62.87	7.84	20.0	523.0	550.84	0.20	0.04	1323.5	0.30	0.02
Flare G,WI=40.82	7.84	20.0	633.3	661.14	0.30	0.05	1378.5	17.30	1.25
NG	7.84	20.0	521.8	549.64	0.49	0.09	1301.0	26.70	2.05

*continued

Mix 1,WI=50.64	7.84	20.0	526.6	554.44	0.17	0.03	1321.7	11.20	0.85
Mix 2,WI=51.07	7.84	20.0	535.0	562.84	0.36	0.06	1321.8	2.90	0.22
Mix 3=WI=51.17	7.84	20.0	521.7	549.54	0.06	0.01	1293.1	14.30	1.11
Mix 4,WI=52.13	7.84	20.0	517.9	545.74	0.24	0.04	1307.7	4.70	0.36
Mix 4,10% exs air	7.84	20.0	481.6	509.44	0.19	0.04	1309.2	12.6	1.0
Mix 4,0% exs air	7.84	20.0	437.8	465.64	0.1	0.02	1309.5	10.3	0.8
Mix 5,WI=51.96	7.84	20.0	522.3	550.14	0.35	0.06	1309.6	42.10	3.21
Mix 6,WI=52.71	7.84	20.0	525.5	553.34	0.72	0.13	1330.9	6.50	0.49